https://doi.org/10.5194/egusphere-2024-1942
Preprint. Discussion started: 17 July 2024
© Author(s) 2024. CC BY 4.0 License.

Stable iron isotope signals indicate a “pseudo-abiotic" process driving deep iron release in methanic sediments

Susann Henkel[1], Bo Liu[1], Michael Staubwasser[2], Simone A. Kasemann[3,4], Anette Meixner[3,4], David Aromokeye[5], Michael W. Friedrich[3,5], and Sabine Kasten[1,3,4]

[1] Alfred Wegener Institute Helmholtz Centre for Polar and Marine Research, Am Handelshafen 12, 27570 Bremerhaven, Germany
[2] University of Cologne, Institute of Geology and Mineralogy, Zülpicher Str. 49a, 50674 Köln, Germany
[3] MARUM – Center for Marine Environmental Sciences, University of Bremen, Leobener Str. 8, 28359 Bremen, Germany
[4] Faculty of Geosciences, University of Bremen, Klagenfurter Strasse, 28359 Bremen, Germany
[5] Faculty of Biology/Chemistry, University of Bremen, James-Watt-Straße 1, 28359 Bremen, Germany

Correspondence to: Susann Henkel (susann.henkel@awi.de)

Abstract. The low $\delta^{56}Fe$ values of dissolved iron liberated by microbial iron reduction are characteristic for shallow subsurface sediments and benthic Fe fluxes into the water column. Here, we decipher whether stable Fe isotope signatures in pore water and the respective solid-phase sediment samples are also useful to unravel the processes driving Fe liberation in deeper, methanic sediments. We investigated the fine-grained deposits of the Helgoland mud area, North Sea, where Fe reduction in the methanic subsurface sediments was previously suggested to be coupled to methanogenic fermentation of organic matter and anaerobic methane oxidation. In the evaluated subsurface sediments, a combination of iron isotope geochemistry with reactive transport modelling for the deeper, methanic sediments hints, unsurprisingly, towards a combination of processes affecting the stable isotope composition of dissolved iron. However, the dominant process releasing Fe at depth does not seem to lead to notable iron isotope fraction. Under the assumption that iron reducing microbes generally prefer isotopically light iron, the deep Fe reduction in this setting therefore appears to be “pseudo-abiotic”: If fermentation is the main reason for Fe release at depth, the fermenting bacteria transfer electrons directly or indirectly to Fe(III), but our data does not indicate notable related isotopic fractionation. Our findings strongly contribute to the debate on the pathway for deep Fe^{2+} release by showing that the main underlying process is mechanistically different to the microbial Fe reduction dominating in the shallow sediments and encourages future studies to focus on the fermentative degradation of organic matter as a source of iron in methanic sediments.

1 Introduction

Iron reduction in coastal and marine sediments plays an important role for the degradation of organic matter, the transformation and cycling of carbon species and for benthic nutrient release into the water column (e.g., Baloza et al., 2022; LaRowe and Van Capellen, 2011; Lovley and Phillips, 1986; Thamdrup et al., 1994; Zhou et al., 2023; 2024). Multiple studies,

https://doi.org/10.5194/egusphere-2024-1942
Preprint. Discussion started: 17 July 2024
© Author(s) 2024. CC BY 4.0 License.

e.g. Henkel et al. (2016; 2018), Johnson and Beard (2005), Severmann et al. (2006), Staubwasser et al. (2006), showed that the difference in the isotopic composition of solid Fe(III) and dissolved Fe(II) in shallow marine sediments is similar to the fractionation related to dissimilatory iron reduction (DIR): based on pure culture studies, dissimilatory iron reducing microorganisms (e.g., *Shewanella* spp.) favour the light iron isotope ^{54}Fe, which is therefore preferentially released into pore water while the ferric substrate becomes isotopically heavier (e.g., Beard et al., 1999; 2003a; Johnson et al., 2004; 2005). Part of the microbially liberated (isotopically light) Fe(II) is adsorbed onto the oxide surface and in isotopic exchange with the heavier reactive Fe(III) layer of the oxide. The resulting fractionation (combining DIR and the electron and atom exchange) $\Delta^{56}Fe_{Fe(II)diss\text{-}Fe(III)}$ is up to -3‰ (e.g., Crosby et al. 2005; 2007). Iron isotopes, expressed as $\delta^{56}Fe$ (‰), are thus considered as a tool for assessing the role of microbial iron reduction (MIR) for the mineralization of organic matter and for tracing benthic iron fluxes into the water column (e.g., Conway and John, 2014; Homoky et al., 2009; Severmann et al. 2006, 2010; Sieber et al., 2021). Here, we aim to evaluate whether pore-water and solid-phase Fe isotope signatures are also useful to unravel the processes driving Fe reduction in deeper sediments below the sulfate-methane-transition (SMT) that is frequently observed in freshwater, brackish, and marine depositional environments (e.g., Egger et al., 2017; Hensen et al., 2003; Kasten et al., 1998; März et al., 2008; Oni et al., 2015a; Riedinger et al., 2005; 2010; 2014; Segarra et al., 2013; Sivan et al., 2011; Wersin et al., 1991). The responsible processes are not entirely understood so far. Most of the sites at which this "deep Fe reduction" occurs, are in high deposition areas characterized by a rapid transition of Fe (oxyhydr)oxides through the upper zone of Fe reduction and the following sulfidic interval into methanic, non-sulfidic sediments (e.g., Aromokeye et al., 2020; 2021; Oni et al., 2015a; Riedinger et al., 2005). Dissolved Fe^{2+} concentrations typically increase below the sulfidic interval surrounding the SMT and may reach several hundreds of micromolar, often exceeding Fe concentrations in the upper ferruginous zone close to the sediment surface (e.g., Riedinger et al., 2005; 2014; 2017).

There is a variety of possible biotic and abiotic pathways for deep Fe reduction. Biotic pathways include continuing DIR by use of organic or inorganic electron donors (e.g., Lovley, 1991; Lovley et al., 1989; Roden and Lovley, 1993), organoclastic fermentative Fe reduction (e.g., Lehours, 2010; Lovley and Phillips, 1986), Fe reduction coupled to ammonium oxidation (Bao and Li, 2017), and Fe-coupled anaerobic oxidation of methane (Fe-AOM) (e.g., Aromokeye et al., 2020; Beal et al., 2009; Riedinger et al., 2014; Sivan et al., 2011). It was furthermore discussed whether Fe^{2+} release can also be linked to iron oxide

https://doi.org/10.5194/egusphere-2024-1942
Preprint. Discussion started: 17 July 2024
© Author(s) 2024. CC BY 4.0 License.

reduction by methanogens that can perform Fe-AOM (Yu et al., 2022) or switching between methane generation and Fe reduction (Eliani-Russak et al., 2023; Sivan et al., 2016). In contrast, Fe reduction and potentially also Fe^{2+} liberation can occur (largely) abiotically by reactions with inorganic compounds such as FeS or FeS_2 (Bottrell et al., 2010; Mortimer et al., 2011) and hydrogen sulfide (sulfide oxidation by reduction of Fe(III), e.g., Canfield, 1989; Holmkvist et al., 2011; Pyzik and Sommer, 1981; Riedinger et al., 2010; Thamdrup et al., 1993) as well as by reactions with organic molecules (e.g., oxalate), which themselves might be produced by microbial activity (e.g., Burdige, 1993; Ionescu et al., 2015 and references therein). Recently, Aromokeye et al. (2021) suggested that Fe reduction in methanic sediments of the North Sea occurs concomitantly with the use of crystalline Fe oxides as conduits for interspecies electron transfer between fermentative bacteria and methanogens (methanogenic benzoate fermentation). The mechanistic details of this process are still to be solved. Clearly, abiotic and biotic reactions of Fe in marine sediments are closely interrelated with each other. Moreover, all of them are directly or indirectly linked to the biogeochemical cycling of C and S. In order to fully assess these interlinks, and in particular to determine their relevance for methane generation and/or consumption, we require a better understanding of deep Fe reduction pathways in natural settings and their dependence on environmental conditions. A differentiation between abiotic and biotic Fe reaction pathways - in particular in methanic environments - would furthermore be of interest for studying life in extreme environments such as the sedimentary deep biosphere, where the availability of degradable organic matter and electron acceptors yielding high standard free energies is often strongly limited (e.g., Heuer et al., 2017; D'Hondt et al., 2004). Here, we investigate whether combined pore-water and solid-phase stable Fe isotope signatures can be used to differentiate between biotic and abiotic Fe reduction pathways in methanic sediments. A similar approach for assessing the dominance of Fe-S reactions over MIR and vice versa using Fe isotopes was successfully applied in shallow sediments of the continental margin off California (Severmann et al., 2006). We also specifically investigate the Fe isotopic signals of crystalline Fe oxides, including magnetite, because for the site investigated here these minerals were found to stimulate deep Fe release based on their conductivity (Aromokeye et al., 2021).

To our knowledge, there are only two studies so far focussing on Fe reduction in methanic sediments that also include pore water Fe isotope data: Sivan et al. (2011) proposed the occurrence of Fe-AOM in sediments of Lake Kinneret (Israel) and showed a light isotopic composition of pore water Fe^{2+} (~ -2‰) in the respective interval. A recent study on very old and

https://doi.org/10.5194/egusphere-2024-1942
Preprint. Discussion started: 17 July 2024
© Author(s) 2024. CC BY 4.0 License.

compacted sediments of the Nankai Trough off Japan (IODP Site C0023) showed that extremely negative pore-water $\delta^{56}Fe$ values of up to -5.9‰ most likely derive from a combination of MIR and Rayleigh fractionation where $^{56}Fe^{2+}$ is preferentially adsorbed onto mineral surfaces (Köster et al., 2023).

Despite the lack of data concerning Fe isotope fractionation during biotic reduction pathways other than DIR, we assume that microbially mediated Fe liberation in methanic sediments similarly results in a preferential release of $^{54}Fe^{2+}$ and, thus, shifts pore-water $\delta^{56}Fe$ towards negative values. Furthermore, we hypothesize that the microbial utilization of a specific Fe (oxyhydr)oxide pool results in a relative enrichment of ^{56}Fe in the remaining substrate, which is detectable by a combination of sequential solid-phase Fe extractions and $\delta^{56}Fe$ analyses after Staubwasser et al. (2006) and Henkel et al. (2016; 2018). We present a compilation of inorganic geochemical data including pore-water and bulk solid-phase geochemistry, iron monosulfide and pyrite extractions as well as $\delta^{56}Fe$ in pore water and reactive Fe pools in order to assess sources and sinks of dissolved iron in the methanic sediments of the Helgoland mud area (HMA, German Bight, North Sea). We exemplarily tested if the $\delta^{56}Fe$ data, in combination with geochemical transport reaction modelling and the information from the previous microbiological studies, can be used to trace and explain the contributions of Fe reduction processes at different depths in the sediment column and discriminate abiotic and biotic reduction pathways.

2 Materials and Methods

2.1 Study Area

The Helgoland mud area (HMA, Fig. 1) is a halotectonic depression in the German Bight filled with Holocene mud that is mostly discharged by the rivers Elbe and Weser (e.g., Hertweck, 1983; Irion et al., 1987). It is one of the few depocenters of fine-grained and organic-carbon-rich sediments in the German Bight, extends over ~500 km², and has an average water depth of 20 m (Hebbeln et al., 2003). Irion et al. (1987) described that between 10,000 and 8,000 yrs BP the Elbe estuary was located at the present position of the HMA and that the old glacial relief formed a barrier towards the north that allowed the mud deposition in a comparatively protected bight. According to Irion et al. (1987), this protective barrier was destroyed about 3,000 to 2,000 yrs BP due to wave and tide activities. High sedimentation rates of more than 13 mm/yr characterized the HMA between ~1,250 - 700 yrs BP and were attributed to the disintegration of the Island of Helgoland in the Middle Ages (Hebbeln

https://doi.org/10.5194/egusphere-2024-1942
Preprint. Discussion started: 17 July 2024
© Author(s) 2024. CC BY 4.0 License.

et al., 2003). The reduction of sedimentation rates to <3 mm/yr after ~700 yrs BP was linked to a slowdown of the disintegration of the island and/or a change of the deposition location (Hebbeln et al., 2003). The high sedimentation rates that prevailed in the region of the HMA before 700 yrs BP led to a fast burial and good preservation of reactive Fe (oxyhydr)oxides, which is a prerequisite of deep Fe reduction.

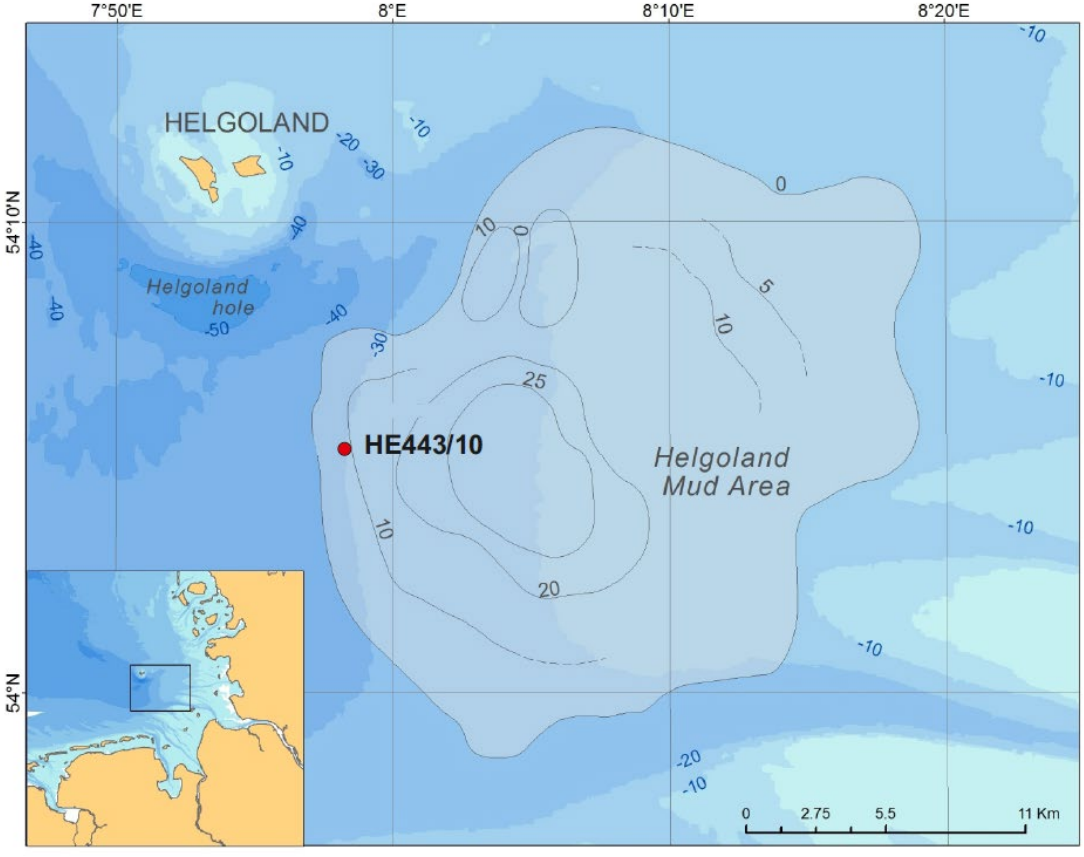

Figure 1: Position of cores collected during RV Heincke expedition HE443. Contour lines indicate the thickness of the mud in m after Hebbeln et al. (2003).

Previous investigations in the western HMA showed a deep Fe release from sediments below the sulfidic zone. The studies by Oni et al. (2015a) and Aromokeye et al. (2020; 2021) demonstrated that the Fe release is directly or indirectly related to microbial activity. Oni et al. (2015a) found a correlation of dissolved iron (Fe_{diss}) concentrations with the abundance of *Atribacterota* (formerly known as Candidate phylum JS1), methanogens, and *Methanohalobium*/ANME-3 related archaea. It

https://doi.org/10.5194/egusphere-2024-1942
Preprint. Discussion started: 17 July 2024
© Author(s) 2024. CC BY 4.0 License.

was therefore suggested that these microbes could be involved in deep Fe reduction, possibly via a simultaneous occurrence of methanogenesis and Fe-mediated AOM. Aromokeye et al. (2020) performed an incubation experiment on sediment material from the same site as ours (parallel core, site HE443/10). Aromokeye et al. (2020) could detect Fe-AOM in slurries from the methanic zone, in particular in long-term incubations (250 days) amended with synthetic Fe oxides. Dissolved Fe was, however, also released from sediments of the methanic zone when those were incubated with N_2 in the headspace (so unrelated to methane oxidation), irrespective of synthetic Fe oxide addition. The authors therefore concluded that there are additional processes for deep Fe_{diss} generation that are directly linked to OM degradation. One of these pathways was later suggested to be coupled to the fermentation of complex organic matter (Aromokeye et al., 2021).

2.2 Sediment and pore-water sampling

The data shown here derive from a multiple corer (MUC) deployment and a gravity core (GC) collected during RV HEINCKE cruise HE443 in April 2015 (MUC: 54°05.14' N, 7°58.15' E, GC: 54°05.19' N, 7°58.21' E, water depth 30 m, Fig. 1). The GC, HE443/10-3, had a length of 488 cm. As surface sediment is usually lost during GC coring, the data of the MUC, HE443/10-2, were used to fit GC pore-water data and calculate actual sediment depths for GC samples.

Directly after coring, the GC was cut into 1 m segments. Samples for methane (CH_4) analysis (3 ml of sediment) were taken immediately at the segment ends and stored in headspace vials pre-filled with 20 ml of a saturated NaCl solution containing NaN_3. The vials were sealed and stored at 4°C until analysis. The GC segments were further sampled through small windows cut into the liner. First, additional CH_4 samples were collected. Then, pore water was extracted at 20 cm intervals using rhizons with an average pore size of 0.1 µm (Seeberg-Elverfeldt et al., 2005). The first ~1.5 ml of collected pore water were discarded. Afterwards, 1.5 ml were collected and mixed with zinc acetate (ZnAc) for onshore sulfide measurements, 2 ml were stored in glass vials without headspace for dissolved inorganic carbon (DIC) analysis, 400 µl were diluted 1:10 with a NaCl solution for ammonium (NH_4) and phosphate (PO_4^{2-}) analyses, and ~1 ml was stored for onshore sulfate (SO_4^{2-}) and chloride (Cl^-) measurements. After collection of pore water for the above-mentioned parameters, new syringes pre-filled with 50 µl of concentrated double-distilled HNO_3 were attached to the rhizons and another 1-2 ml were collected for cation analysis. Pore-water aliquots were all stored at 4°C. To maximize the sample volume, pore water for $\delta^{56}Fe$ analyses was collected in between the depths sampled for all other pore water parameters, also in 20 cm intervals. However, we only processed every second to

https://doi.org/10.5194/egusphere-2024-1942
Preprint. Discussion started: 17 July 2024
© Author(s) 2024. CC BY 4.0 License.

third sample and based the sample selection on the Fe_{diss} profile shape with a higher resolution close to reaction fronts and a lower resolution where Fe_{diss} shows a rather linear gradient. Those samples were collected in pre-cleaned PP vials: one day 3% ELMA70 (an alkaline detergent), one day deionised water, seven days 0.3 M HCl, three days ultra-pure water. All $\delta^{56}Fe$ samples were acidified with double-distilled HCl. Solid-phase samples were collected using cut-off syringes, tightly sealed, and stored at -20°C in Ar-filled, gas-tight glass containers. Six months after coring, the GC was cut open and X-radiographs were produced at the Alfred Wegener Institute Helmholtz Centre for Polar and Marine Research in Bremerhaven (AWI).

We collected three parallel MUCs during one deployment at the same location that was cored with the GC: one for pore-water $\delta^{56}Fe$ sampling, one for solid phase analyses, and one for all other parameters mentioned above for the GC except for CH_4. Pore-water sampling was conducted as described above, but in 1 cm intervals down to a depth of 10 cm and every 2 cm further below. Solid-phase samples were gained by slicing the MUC core in 1-2 cm intervals. These samples were all treated as previously described.

Both, the MUC and the GC core, HE443/10-2 and -3, consisted of dark to very dark grey mud. The GC that was cut open onshore showed bioturbation structures over the whole core length. Only in the following intervals (core depths), sediment lamination was still largely intact: 20 to 27 cm, 121 to 135 cm, 190 to 195 cm, 238 to 264 cm, 273 to 278 cm, 311 to 326 cm, 340 to 388 cm, 441 to 447 cm. Layers and lenses of silty material are present at 60 cm, 275 cm, 350 to 360 cm, and 370 to 380 cm. X-radiographs of the core are accessible in the PANGAEA database (doi: xxx).

2.3 Pore-water analyses

The following pore-water analyses were conducted at the AWI: DIC, NH_4, and PO_4 were measured directly after the cruise using a QuAATro SEAL nutrient analyzer. The methods were used as described in the user handbook (Q-067-05, Q-080-06, Q-064-05) and are based on Stoll et al. (2001) (for DIC), Kerouel and Aminot (1997) (for NH_4) and on the complex formation of PO_4^{3-} with ammonium molybdate, respectively. The pH value was measured in sampled pore water using a pH electrode and a WTW pH meter. Cation concentrations were determined by inductively coupled plasma – optical emission spectrometry (Iris Intrepid II ICP-OES). Dissolved sulfide ($\sum H_2S = H_2S + HS^- + S^{2-}$) was analyzed using the methylene blue method (Cline, 1969). Sulfate and chloride were measured in 1:50 dilution using a Metrohm Compact IC 761 ion chromatograph. Headspace gas for CH_4 analysis was injected into a Thermo Finnigan TRACE GC equipped with a packed column and an integrated flame

https://doi.org/10.5194/egusphere-2024-1942
Preprint. Discussion started: 17 July 2024
© Author(s) 2024. CC BY 4.0 License.

ionization detector (FID). Methane concentrations were calculated under consideration of an average porosity of 0.7, determined based on the water content of sediment samples and an estimated average grain density of 2.6 g cm^{-3}.

Pore-water processing for $\delta^{56}Fe$ analysis was conducted at the University of Cologne: Fe was first pre-concentrated and extracted from the salt matrix using the NTA Superflow resin as described by Henkel et al. (2016; 2018). Subsequently, samples were further purified by anion exchange chromatography using 150 µl Dowex 1X8 200-400 resin. All columns and vials used during the processing were pre-cleaned with ELMA70 and diluted HCl as described above for the PP sampling vials. The purified Fe samples were matched to a concentration of 0.2 ppm and introduced into a ThermoFinnigan Neptune multicollector-ICP-MS equipped with an Aridus desolvating nebulizer system at the Steinmann Institute in Bonn. We applied the standard-sample bracketing method with IRMM-014 (e.g., Schoenberg and von Blanckenburg, 2005). Data are reported as: $\delta^{56}Fe\ [‰] = (^{56}Fe/^{54}Fe_{sample})/(^{56}Fe/^{54}Fe_{IRMM\text{-}014}) - 1] * 1000$.

Details concerning the instrumental setup can be found in Henkel et al. (2016; 2018). We monitored the measurement trueness of the isotopic analyses by use of the reference material JM, a solution produced from an Fe wire supplied by Johnson & Matthey. The measured value was 0.49 ± 0.26‰ (n=15, 2SD) and overlapped within uncertainty with previously published values (0.42 ± 0.05‰, Schoenberg and von Blanckenburg, 2005; 0.46 ± 0.20‰, Walczyk and von Blanckenburg, 2005; 0.35 ± 0.14‰, Weyer and Schwieters, 2003). The uncertainty of a single measurement (2SD of one block of 20 measurement cycles) was between 0.07 and 0.14‰. Processing and analysis of two duplicate samples resulted in $\delta^{56}Fe$ values within the uncertainties (2 SD) of the respective single measurements. Pore-water $\delta^{56}Fe$ values were analysed using a Keeling plot that is traditionally used for carbon isotope mixing (Keeling, 1958; Pataki et al., 2003). Details are given in section 4.2.

2.4 Solid-phase analyses

The bulk elemental composition of the sediment was determined by total digestion of about 50 mg of freeze-dried and ground sediment in a mixture of concentrated acids (3 ml HCl, 2 ml HNO_3, and 0.5 ml HF). The digestion was carried out in a CEM Mars Xpress microwave system at AWI. After evaporation of the acids, the residue was dissolved in 1 M HNO_3 and measured by ICP-OES. Recoveries of processed NIST SRM2702 reference material (n=5, uncertainty given as 2 SD) were 100.2 ± 0.8% for Fe, 98.1 ± 2.4% for Mn, 101.5 ± 2% for Ca, and 93.8 ± 2.8% for Al. Total Fe contents were published by Aromokeye et al. (2020) and are available under https://doi.org/10.1594/PANGAEA.893760.

https://doi.org/10.5194/egusphere-2024-1942
Preprint. Discussion started: 17 July 2024
© Author(s) 2024. CC BY 4.0 License.

Sequential Fe extractions were performed after Poulton and Canfield (2005): ~50 mg of dry sediment were suspended in always 5 ml of a) $MgCl_2$ for adsorbed Fe, b) Na-acetate for Fe-carbonates and surface-reduced Fe(II), c) hydroxylamine-HCl for easily reducible Fe-oxides (ferrihydrite, lepidocrocite), d) Na-dithionite/citrate for reducible Fe-oxides (goethite and hematite) and e) ammonium oxalate/oxalic acid for magnetite. In contrast to the method by Poulton and Canfield (2005), we used a lower concentration of citrate for the dithionite extraction since citrate hinders Fe precipitation during subsequent sample purification for δ^{56}Fe analysis (Henkel et al., 2016). Instead, we performed the extractions under anoxic conditions. Aliquots of all extracts were analyzed by ICP-OES. A separate aliquot of 2 ml of each extract was processed for δ^{56}Fe analysis following the protocol by Henkel et al. (2016). The purified Fe samples were matched to a concentration of 0.5 ppm and were analyzed using the ThermoScientific Neptune plus MC-ICP-MS of the Isotope Geochemistry Group at MARUM-Centre for Marine Environmental Sciences, University of Bremen. The MC-ICP-MS was equipped with a SSI dual cyclonic spray chamber, a low flow 50 µl PFA nebulizer and a Ni skimmer cone (x-type). Samples were measured using the standard-sample bracketing with certified reference material IRMM-014. All ^{54}Fe data were Cr-corrected based on measurements of ^{52}Cr. In addition, all data were blank-corrected and samples were analysed in random order. The standard JM (see above) was analysed after each block of three samples. Samples bracketed by JMs that did not fall into the target range of 0.42 ± 0.05‰ were repeatedly measured. The repeatability precision resulting from up to 6 replicate sample measurements (not including replicate processing) was better than 0.34‰ (2SD) and on average 0.11‰. The intermediate precision of JMs was 0.44 ± 0.15‰ (n=151, 2SD).

Acid volatile sulfide (AVS; mostly iron monosulfides) and chromium reducible sulfide (CRS; mostly pyrite, but potentially also elemental sulfur) were extracted at AWI by hot digestion using 6 M HCl and a chromous chloride solution, respectively (Canfield et al., 1986; Praharaj and Fortin, 2003; Wieder et al., 1985). Extracted sulfur was trapped in a silver nitrate solution as Ag_2S. After filtration, the dry masses of the precipitates were converted into FeS and FeS_2 contents based on stoichiometry. Replicate analysis of an inhouse standard (core catcher sediment of GC HE443/077) revealed good reproducibility of the extractions with AVS contents of 0.11 ± 0.01 wt% and pyrite contents of 1.03 ± 0.05 wt% (n=7).

https://doi.org/10.5194/egusphere-2024-1942
Preprint. Discussion started: 17 July 2024
© Author(s) 2024. CC BY 4.0 License.

On freeze-dried, powdered, and homogenized sediment samples, the total carbon (TC) contents were determined using a CNS (Elementar Vario EL III) analyzer. Total organic carbon (TOC) contents were measured with a carbon–sulfur analyzer (CS-2000, ELTRA) after removal of inorganic carbon with HCl.

2.5 Model setup and parameterization

A reactive transport model was used in order to (1) exemplarily assess if the measured pore-water Fe and δ^{56}Fe profiles at site HE443/10 can be reproduced based on Fe reactions that are known to occur (MIR and Fe sulfide formation) and (2) to delineate how sensitive the pore-water Fe and δ^{56}Fe profiles are with respect to different reaction rate contants *k* and related fractionation factors. To keep this approach as simple and straight-forward as possible, we only included the most basic and presumably dominant reactions that are known to affect the dissolved Fe pool and its isotopic composition: organoclastic DIR, reaction of hydrogen sulfide with Fe(III) to Fe sulfide, and the precipitation of Fe sulfides by counter-diffusion of pore water Fe^{2+} and HS^- (R1-R3, Table S1):

$$CH_2O + 4\ Fe(OH)_3 \rightarrow HCO_3^- + 4\ Fe^{2+} + 3\ H_2O + 7\ OH^- \quad (R1)$$

$$Fe(OH)_3 + 2\ HS^- \rightarrow FeS_2 + 2\ OH^- + H_2O + 0.5\ H_2 \quad (R2)$$

$$Fe^{2+} + 2\ HS^- \rightarrow FeS_2 + H_2 \quad (R3).$$

We are aware that we miss some reactions in the model that might play a role as well, e.g., siderite or vivianite precipitation, Fe-AOM, and re-oxidation of sulfide by Fe(III). Furthermore, R3 is actually not a single reaction, but includes the formation of monosulfide (FeS) and (in a second step) the transformation of FeS into FeS_2, where the latter reaction can happen abiotically, but can also be driven by microbes (Thiel et al., 2019). Our approach is basically backwards as we check whether we can reproduce the profile shapes of dissolved Fe and the respective δ^{56}Fe values from the deep Fe source to the sink at the sulfidization front sufficiently well by just including these basic reactions or whether we miss a reaction that would be needed to explain the measurements. With regard to siderite and vivianite formation, a calculation with PHREEQC (see section 2.6) in fact indicates oversaturation below the SMT at site HE443/10-3. Nevertheless, we chose to neglect these reactions in the model as the specific contributions are unclear (siderite and vivianite) or respective Fe fractionation factors are unknown (vivianite). We discuss, however, how particularly siderite precipitation could affect our results, e.g., Fe extraction data and the dissolved Fe isotope profile in sections 4.1 and 4.2. Since we were primarily interested in the deep Fe reduction, modelling

https://doi.org/10.5194/egusphere-2024-1942
Preprint. Discussion started: 17 July 2024
© Author(s) 2024. CC BY 4.0 License.

was confined to the sediment interval between 70 cm (sulfide peak) and 450 cm (end of core). We disregarded all the reduction and oxidation processes above the sulfide peak as they are irrelevant for the expression of aqueous $\delta^{56}Fe$ below the sulfidic zone. This is because Fe^{2+} is completely removed within the sulfidic zone due to the reaction with HS^-.

The reaction rates were obtained according to the concentrations of the reacting species. For example, R2 and R3 approach zero when HS^- is depleted. The following transport-reaction equations for Fe^{2+} and HS^- were used:

$$\frac{\partial[Fe^{2+}]}{\mathrm{dt}} = -\omega\frac{\partial[Fe^{2+}]}{\partial z} + \frac{D_{Fe^{2+}}}{\tau^2}\cdot\frac{\partial^2[Fe^{2+}]}{\partial z^2} + 4R_1 - R_3 \qquad \text{(Eq. 1)}$$

$$\frac{\partial[HS^-]}{\mathrm{dt}} = -\omega\frac{\partial[HS^-]}{\partial z} + \frac{D_{HS^-}}{\tau^2}\cdot\frac{\partial^2[HS^-]}{\partial z^2} + 2R_2 - 2R_3 \qquad \text{(Eq. 2)}$$

where $[Fe^{2+}]$ and $[HS^-]$ are the concentrations of dissolved iron and sulfide, t is time, ω is the sedimentation rate, z is the depth below seafloor, and D_{Fe2+} and D_{HS^-} are the diffusion constants for dissolved iron and sulfide. The applied sedimentation rate (0.16 cm yr^{-1}) derives from Hebbeln et al. (2003). Diffusion constants for seawater at pore-water temperature (4°C) are from Boudreau (1997) (D_{Fe2+} = 0.0116 m^2/yr and D_{HS-} = 0.0306 m^2/yr). A constant porosity (ϕ) of 0.7 was assumed and the tortuosity (τ) in Eq. (1) and (2) was calculated according to Boudreau (1996) as $\tau^2 = 1 - \ln(\phi^2)$. Although the organic matter (OM) degradation rate constant k_1 decreases with burial depth (Arndt et al., 2013), its variation is low below the SMT under high burial rate conditions. For simplicity, the Fe reduction rate coupled with OM degradation is assumed to follow the first order decay model (E1, see Table S1). The pool of reducible Fe-oxides is set to not be limiting and based on the data gained from sequentially extracted Fe and its $\delta^{56}Fe$ composition was kept at a constant value of 0.0‰ (see Results). Within the sulfidic zone there is no free Fe^{2+} (assumption: 0.01 µM at the upper boundary) and all Fe^{2+} released from the abiotic reaction with HS^- (sulfide oxidation by reduction of iron (oxyhydr)oxides) is assumed to be immediately converted to pyrite (R2). Due to the complete turnover of released Fe^{2+} it is reasonable to assume that there is no related isotopic fractionation (α_2 = 1.000). During Fe sulfide formation where Fe^{2+} and HS^- counter-diffuse, we applied the kinetic fractionation factor α_3 ($\alpha_{Fepy\text{-}Fe(II)diss}$) which was set to 0.999, 0.998, and 0.997 to fit the measured data and result in dissolved Fe with an isotopic composition $\delta^{56}Fe_{diss}$ ~0‰ compared to more negative values measured below (see Results and Discussion), where Fe concentrations are higher (upward Fe diffusion). In other words: Fe sulfide formation via the reaction of Fe^{2+} with HS^- preferentially incorporates ^{54}Fe (e.g., Butler et al., 2005; Scholz et al., 2014; Severmann et al., 2006). In addition, in different model runs we applied a fractionation factor α_1 ($\alpha_{Fe(II)diss\text{-}Fe(III)}$) = 0.998, 0.997, and 0.996 for DIR below 70 cm depth in order to reproduce the measured

https://doi.org/10.5194/egusphere-2024-1942
Preprint. Discussion started: 17 July 2024
© Author(s) 2024. CC BY 4.0 License.

pore water $\delta^{56}Fe$ profile. These values are in the range of DIR fractionation factors published by Beard et al. (1999, 2003b), Crosby et al. (2007), Johnson et al., (2005), and Severmann et al. (2006). It is important to note that the factors we apply do not resolve all involved partial fractionation processes, but only the fractionation related to the sum reactions R1 and R3. Our α_1 for example reflects the isotopic difference between solid phase Fe(III) and dissolved Fe(II), but in reality isotopic fractionation happens not only during the microbial Fe reduction and Fe^{2+} release, but also between adsorbed Fe(II) and a reactive solid Fe(III) and adsorbed Fe(II) and the dissolved Fe(II), respectively (Crosby et al., 2005; 2007). Furthermore, we note that it is a valid approach to use *k* as fitting parameter, because for biotic reactions, the rate constant is not only depending on temperature, but also on the abundance and activity of microbes. Typically, this leads to a very large range of constant values. For example, the rate constant was given as 100 and 14800 mM^{-1} yr^{-1} for the same reaction $Fe^{2+} + H_2S \rightarrow FeS$ in Reed et al. (2011a) and Reed et al. (2011b), respectively. In our study, k_2 also depends on the contents of reactive $Fe(OH)_3$, because R2 is generally expressed as $k[Fe(OH)_3][H_2S]$. k_3 combines the fast FeS formation rate constant $k[Fe^{2+}][H_2S]$ and slow FeS_2 rate constant $k[FeS][H_2S]$. All model parameters and boundary conditions are given in Table S2.

2.6 Calculation of saturation indices (SI)

The saturation indices of selected secondary Fe-minerals, namely vivianite and siderite, were calculated using the computer program PHREEQC (Parkhurst and Appelo, 2013). The thermodynamic database 'phreeqc.dat' was used because it has a relatively wide range of aqueous complexation reactions for twenty-five chemical elements, including P and Fe. The input files defined for the geochemical calculations in PHREEQC are based on measured DIC, pH, and the aqueous concentrations of Mg^{2+}, PO_4^{3-}, NH_4^+, SO_4^{2-}, HS^-, Cl^-, Mn^{2+} and Fe^{2+}. NO_3^- was set to zero as it is already depleted close to the sediment surface. Since the redox potential (Eh) is a mandatory input variable for this type of geochemical calculations, but was unavailable, the default values in PHREEQC were used. The effect of Eh on the saturation of vivianite and siderite was insignificant as determined by a sensitivity test. The *in situ* temperature of the pore water was set to 4°C. The concentration of Fe^{2+} within the sulfidic zone was set to 1 µM as the detection limit.

https://doi.org/10.5194/egusphere-2024-1942
Preprint. Discussion started: 17 July 2024
© Author(s) 2024. CC BY 4.0 License.

3 Results

Based on the DIC and SO_4^{2-} profiles of the MUC and GC cores, the core loss during gravity coring was determined to be 16 cm. Core depths of the GC were corrected to sediment depth accordingly.

3.1 Pore-water geochemistry

The pore-water profiles of SO_4^{2-}, HS^-, CH_4 (only end of core segments), DIC, dissolved Fe and Mn of GC HE443/10-3 have been shown earlier in Aromokeye et al. (2020) and are available in the data base PANGAEA (doi: 10.1594/PANGAEA.893766; core depths instead of sediment depths).

The pore water profiles at site HE443/10 indicate ferruginous conditions at 1-2 cm depth. Dissolved Fe concentrations peak at 5 cm with 180 µM and then decrease towards 10 cm depth, where Fe and dissolved sulfide counter-diffuse (Fig. 2). Sulfate shows a kink-shaped profile with a minor decrease from the sediment-water interface to 15 cm depth (25.3 to 24.3 mM) and a steeper gradient further downcore to ~0 mM at 86 cm. Sulfidic conditions prevail between 10 and 100 cm depth. Sulfide concentrations in the pore water peak at ~70 cm depth (0.5 mM), where SO_4^{2-} and CH_4 counter-diffuse. Right below the SMT, CH_4 concentrations increase to ~3 mM and more. Higher values, ≥4 mM, were measured in samples directly taken from ends of core segments during the cutting of the core. At depth, CH_4 concentrations do not significantly increase. Below the sulfidic zone, dissolved Fe (Fe_{diss}) concentrations gradually increase downcore to 400 µM at 350 cm. The concentrations remain at this level further below. The $\delta^{56}Fe_{diss}$ profile shows most negative values at the sediment-water interface (-1.8‰) (Fig. 2). The values increase to about -1‰ at 8 cm depth. There are no $\delta^{56}Fe_{diss}$ values for the sulfidic zone due to absence of Fe_{diss}. Right below the sulfidic zone, where Fe_{diss} concentrations of ~100 µM were detected, $\delta^{56}Fe_{diss}$ is 0‰. As Fe_{diss} concentrations increase further downcore, there is a shift to -1.3‰ at 186 cm followed by a gradual increase of values towards 0‰ at 450 cm, where Fe_{diss} peaks.

https://doi.org/10.5194/egusphere-2024-1942
Preprint. Discussion started: 17 July 2024
© Author(s) 2024. CC BY 4.0 License.

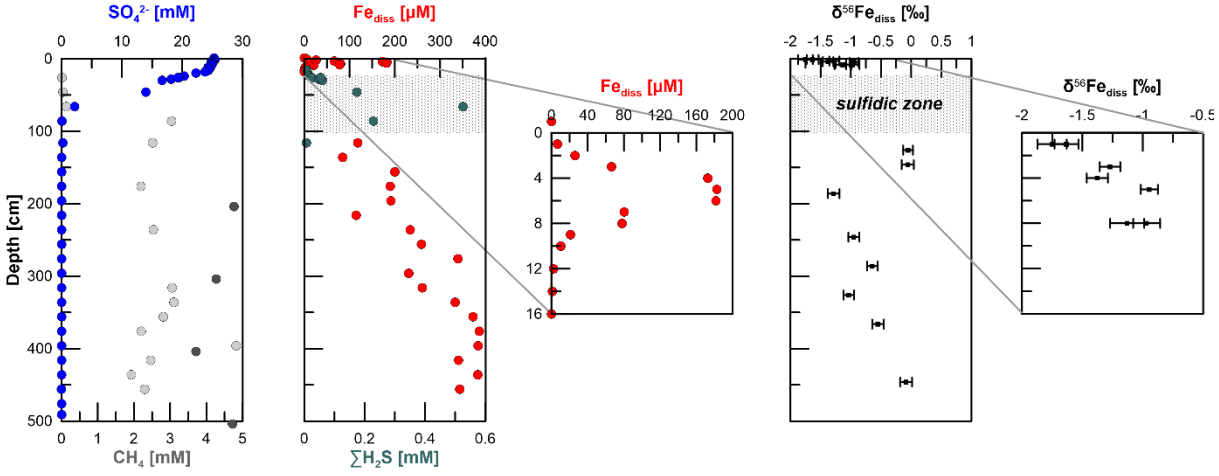

Figure 2: Pore water profiles of SO_4^{2-} and CH_4 at station HE443/10. Dark grey dots of the CH_4 graph indicate samples from ends of core segments. Those concentrations are more reliable compared to the others, as samples were directly taken during cutting of the core segments. The second and third panel show dissolved Fe and H_2S concentrations as well as the stable Fe isotope values of dissolved Fe in the non-sulfidic sediments (uncertainty bars are 2SD). Sulfate, methane (only end of core segments), sulfide and dissolved iron data of the gravity core were published earlier by Aromokeye et al. (2020). In all plots, the grey shaded area indicates the sulfidic interval.

Phosphate concentrations show an increase from 9 µM at 1 cm depth to ~530 µM at 90 cm. Concentrations then decrease gradually to ~250 µM at depth (Fig. 3). Phosphorus concentrations measured by ICP-OES of acidified pore-water aliquots (not shown, but available under xxx) mirror the overall PO_4 profile so that we can exclude a drawdown of PO_4 at depth as a sampling artefact in Fe-rich pore water from below the SMT. Oxidation of samples easily leads to Fe precipitation and PO_4 drawdown due to adsorption.

The Mn pore-water profile shows concentrations of ~50 µM at 3 cm sediment depth. Towards the sulfidic zone, concentrations decrease to zero. A second maximum of Mn concentrations (~200 µM) is located at 200 cm. Down to this depth, the Mn profile shape mirrors the Fe_{diss}, although concentrations are considerably lower. Unlike Fe_{diss}, Mn concentrations then decrease to 15 µM at 415 cm. Towards the end of the core, Mn increases again to 40 µM. Dissolved Ca concentrations how an overall downcore decrease from 9 to 5 mM (Fig. 3). Ammonium concentrations show a steady increase from 45 µM

https://doi.org/10.5194/egusphere-2024-1942
Preprint. Discussion started: 17 July 2024
© Author(s) 2024. CC BY 4.0 License.

at 1 cm depth to 13.8 mM at 300 cm. The concentrations remain at this level for the rest of the core (Fig. 3). pH averages at 7.85 above and at 7.29 below the SMT and DIC increases from 2.5 mM in the bottom water to 66 mM at 476 cm sediment depth (Fig. 3).

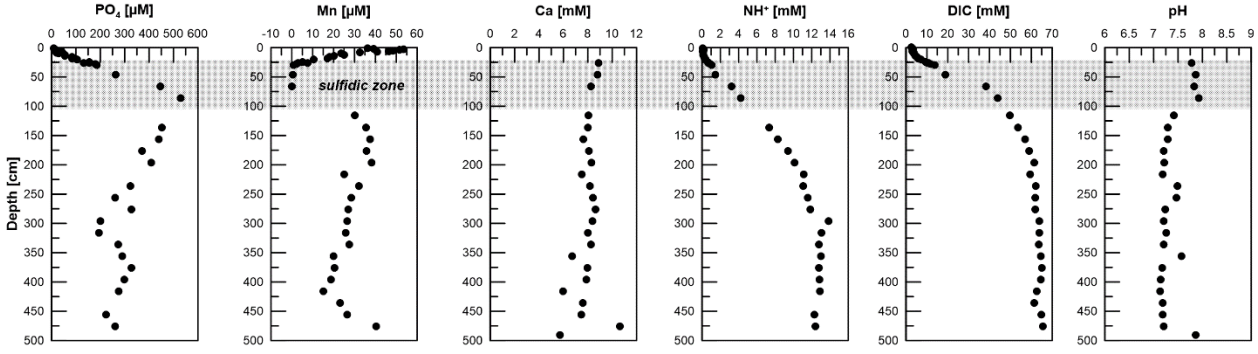

Figure 3: Pore water PO4, Mn, Ca, NH_4^+, DIC, and pH data for site HE443/10. The Mn pore water profile of the gravity core was already published by Aromokeye et al. (2020).

3.2 Solid phase composition

Total Fe contents (Fe_{total}) of GC HE443/10-3 have been shown earlier by Aromokeye et al. (2020) and are available in the PANGAEA database (doi: 10.1594/PANGAEA.893760; with core depths instead of sediment depth). Sequentially extracted Fe data as well as Mn and Al contents are available in PANGAEA (xxx).

Fe_{total} varies between 17 and 42 mg/g (Fig. 4). The Fe/Al ratio (g/g) at Site HE443/10 is between 0.49 and 0.69 (average 0.59) with higher Fe/Al values corresponding to high Fe_{total} contents. According to the sequential extraction data, 16-30% of Fe_{total} are associated with Fe-carbonates, FeS (which is not targeted here, but dissolves in 1 M Na-acetate and was targeted in a separate extraction of Fe sulfides, see below), and Fe-oxides. There is no clear downcore decrease of Fe_{total} or the sequentially extracted Fe pools (Fig. 4). On the contrary, there are intervals of elevated Fe contents at 230-300 cm and below 400 cm, which are reflected by all extracted Fe phases. Only when plotted relative to reactive Fe (sum of Fe extracted by $MgCl_2$, Na-acetate, hydroxylamine-HCl, Na-dithionite/citrate, and ammonium oxalate/oxalic acid), the acetate-leached Fe pool (Fe-carbonates

https://doi.org/10.5194/egusphere-2024-1942
Preprint. Discussion started: 17 July 2024
© Author(s) 2024. CC BY 4.0 License.

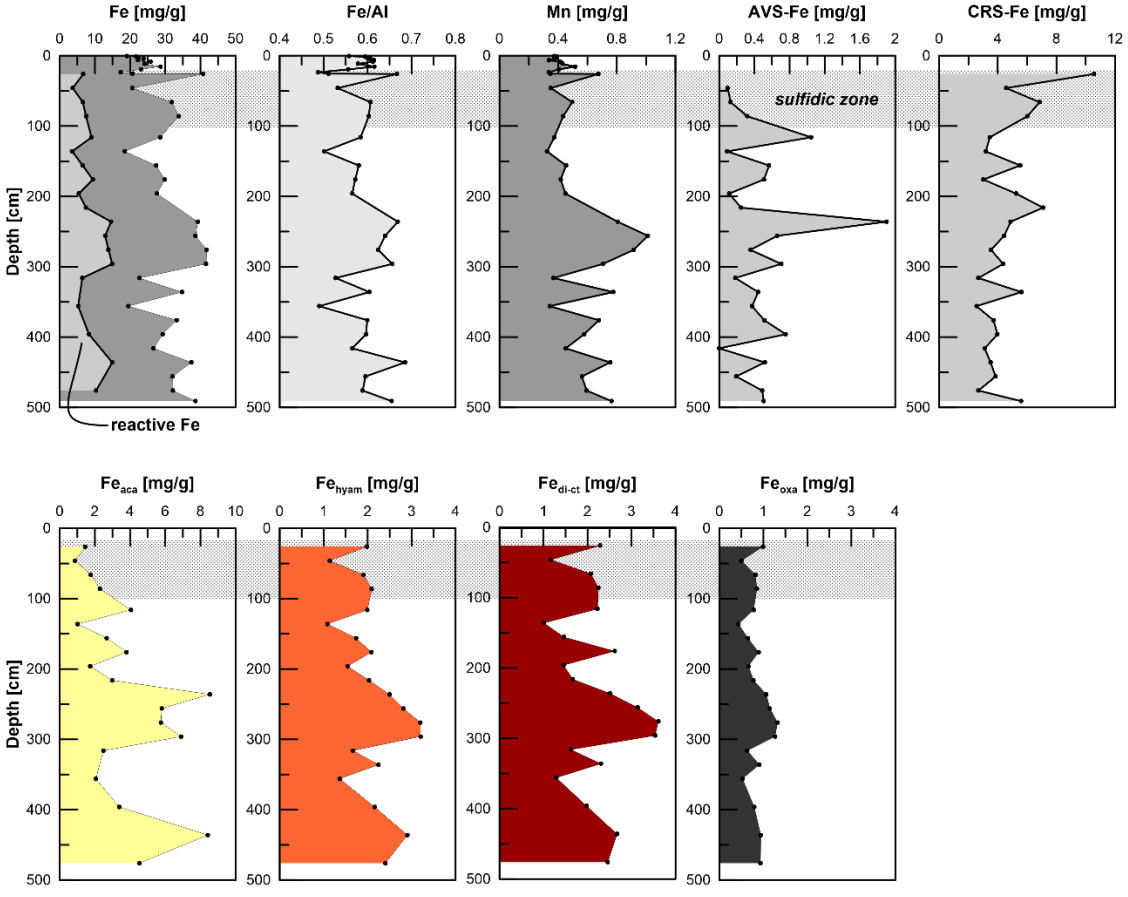

Figure 4: Total and reactive Fe contents, Fe/Al, Mn, AVS-Fe, CRS-Fe and sequentially extracted Fe pools after Poulton and Canfield (2005). Note that reactive Fe is the sum of Fe_{aca} (carbonates, surface-reduced Fe), Fe_{hyam} (amorphous easily reducible oxides), Fe_{dith} (goethite, hematite) and Fe_{oxa} (magnetite). Note that the sequential extraction is not mineral-specific, but operationally defined.

and surface-reduced Fe(II)) shows an overall increase with sediment depth, whereas the other extracted Fe fractions rather show a decrease (Fig. 5). Close to the sediment surface, the composition of reactive Fe is as follows: 20% acetate-leached Fe (Fe_{aca}), 30% hydroxylamine-HCl-leached Fe (Fe_{hyam}), 35% dithionite-leached Fe (Fe_{di-ct}), 15% oxalate-leached Fe (Fe_{oxa}). At 450 cm, the respective values are 50% Fe_{aca}, 20% Fe_{hyam}, 20% Fe_{di-ct}, and 10% Fe_{oxa}. Only the Fe_{aca} pool shows a clear variation in the $\delta^{56}Fe$ composition, where high Fe_{aca} contents correspond to low $\delta^{56}Fe_{aca}$ signals down to -0.54‰ (Fig. 5). Data representation in a Miller-Tans plot (Miller and Tans, 2003; Fig. 6a), which allows assessing even small isotopic variations

https://doi.org/10.5194/egusphere-2024-1942
Preprint. Discussion started: 17 July 2024
© Author(s) 2024. CC BY 4.0 License.

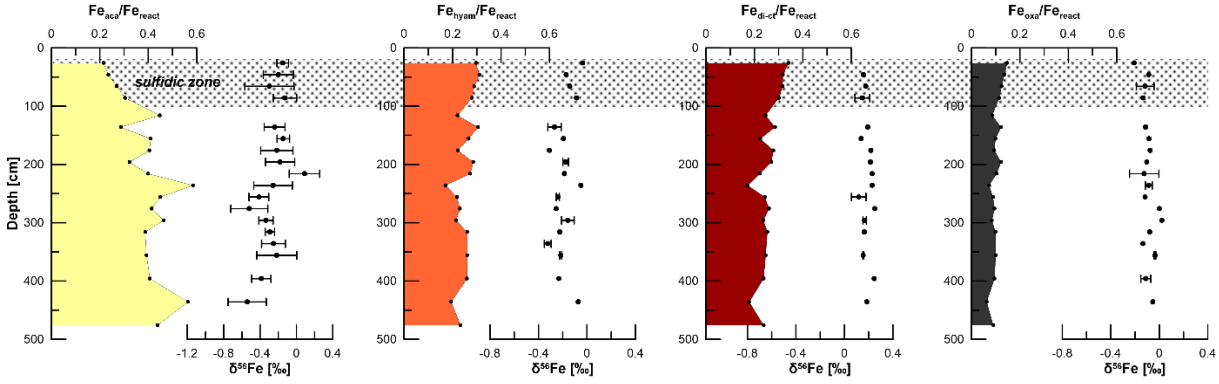

Figure 5: Sequentially extracted Fe pools normalized to the sum of reactive Fe and the respective δ56Fe values. Uncertainty bars are 2SD and given only for samples that were repeatedly analyzed. The grey bar indicates the sulfidic interval.

335

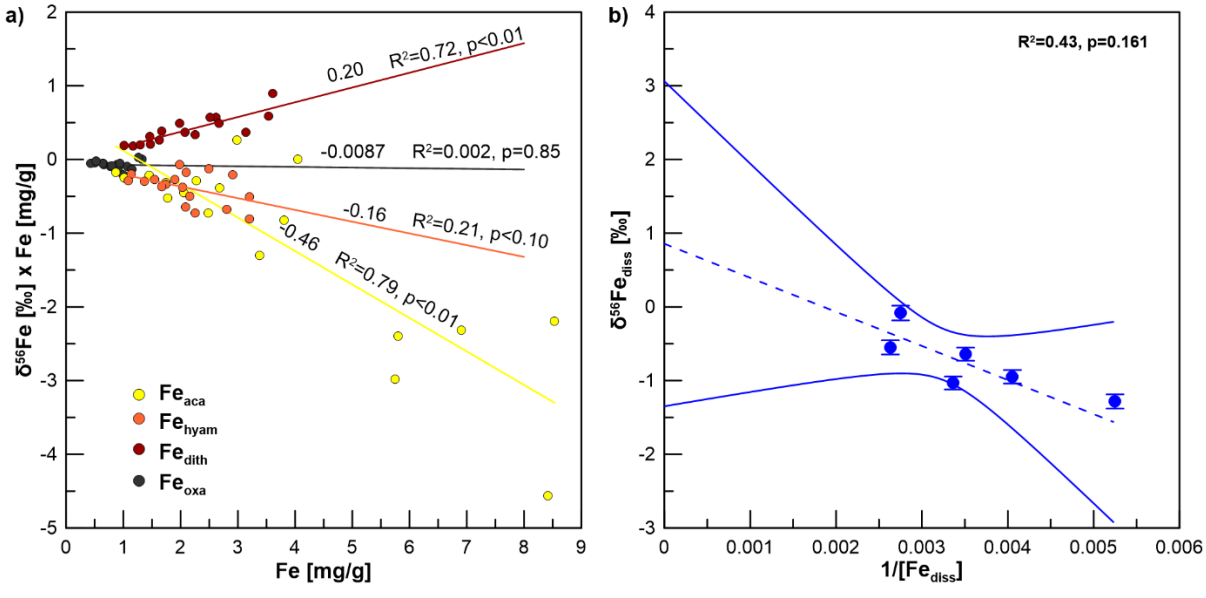

Figure 6: a) Miller-Tans plot for $\delta^{56}Fe$ values of sequentially extracted reactive Fe pools. b) Keeling plot for $\delta^{56}Fe$ values of pore water with 95% confidence interval.

that depend on the size of the respective pool, underlines this relationship with R^2=0.79 ($p<0.01$). The hydroxylamine-HCl-leached pool shows overall negative $\delta^{56}Fe_{hyam}$ values (-0.19 ± 0.17‰, 2SD). As for the Fe_{aca} pool, the Miller-Tans analysis indicates a correlation between Fe_{hyam} content and the isotopic composition (Fig. 6a) with higher contents being related to more

https://doi.org/10.5194/egusphere-2024-1942
Preprint. Discussion started: 17 July 2024
© Author(s) 2024. CC BY 4.0 License.

negative $\delta^{56}Fe_{hyam}$ values. The relationship is, however, less clear (R^2=0.21, p<0.1) and the overall range of $\delta^{56}Fe_{hyam}$ (-0.32 to -0.03‰) considerably smaller compared to Fe_{aca}. $\delta^{56}Fe_{di\text{-}ct}$ values (Fig. 5) range between 0.12 and 0.25‰ (0.19 ± 0.08‰, 2SD). The Miller-Tans plot indicates that there is a slight enrichment of ^{56}Fe in samples that show high $Fe_{di\text{-}ct}$ contents (R^2=0.72, p<0.01) (Fig. 6a). Oxalate-leached Fe shows $\delta^{56}Fe_{oxa}$ values of -0.09 ± 0.10‰ (2SD) and neither a downcore trend (Fig. 5) nor a dependency of $\delta^{56}Fe_{oxa}$ to Fe_{oxa} contents (Fig. 6a).

Total Mn contents in the solid phase range from 0.3 to 1 mg/g, where the overall profile shape is very similar to the distribution of Fe_{total}: Maximum values occur between 200 and 300 cm. Local maxima further downcore coincide with maxima in Fe at 335, 375, 435, and 490 cm.

TOC values range between 0.4 and 1.2 wt% (Fig. 7) and show a strong positive correlation with Fe_{total} (R^2=0.76, p<0.01). As for Fe_{total}, there is no decrease of TOC with depth, but a zone of elevated values between 230 and 300 cm and a trend to higher values (up to 1.2 wt%) towards the end of the core. TIC (data available under xxx) shows similar trends, but values are higher (1.3 to 2.3 wt%) compared to TOC.

Iron sulfides are present as AVS and CRS. Both sulfide pools are not limited to the sulfidic zone (Fig. 4), but occur over the whole gravity core length. AVS peaks at the depth of the current sulfidization front at ~100 cm depth (1 mg/g AVS-Fe). A second maximum of 2 mg/g AVS-Fe appears at 250 cm. CRS is highest at 26 cm depth (10 mg/g CRS-bound Fe), the uppermost sample that was analyzed. The contents decrease towards ~120 cm (3 mg/g CRS-bound Fe) and remain at a level of ~4 mg/g further downcore. AVS is affected by the extraction of Fe-carbonates with Na-acetate (Cornwell and Morse, 1987; Poulton and Canfield, 2005). Based on the separate extraction, the contribution of AVS to the Fe_{aca} pool was calculated to be between 6 and 26% (average 13%). This is particularly important with respect to $\delta^{56}Fe_{aca}$ data. Even though there is no correlation between the AVS contribution to Fe_{aca} (in %) and the respective $\delta^{56}Fe_{aca}$ value (R^2=0.03), $\delta^{56}Fe_{aca}$ should be interpreted with caution as it represents a mixed signal of several (secondary) Fe pools that likely have different isotopic compositions: siderite, Fe monosulfides, and surface-reduced Fe(II) (Crosby et al., 2005; 2007; Henkel et al., 2016).

https://doi.org/10.5194/egusphere-2024-1942
Preprint. Discussion started: 17 July 2024
© Author(s) 2024. CC BY 4.0 License.

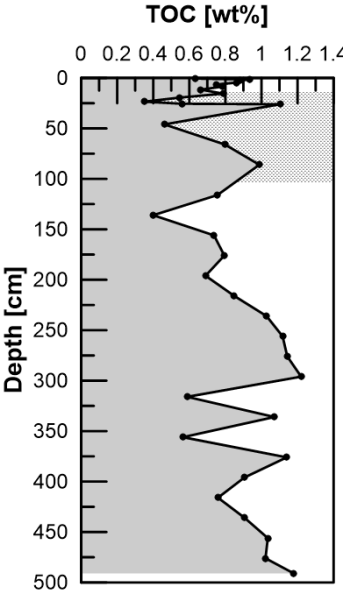

Figure 7: TOC in sediments from Site HE443/10. The grey bar indicates the sulfidic interval.

3.3 Model Results (Transport/Reaction Simulation)

We performed sensitivity tests by applying different fractionation factors α_1 for DIR (R1, k_1 as a function of OM degradation), different reaction rate constants k_2 and fractionation factor α_2=1 for the sulfidization via the reaction of hydrogen sulfide with Fe oxides (R2), and different reaction rate constants k_3 and fractionation factors α_3 for sulfide precipitation via reaction of Fe_{diss} with HS^- (R3). The differences between the measured and calculated concentrations/values C^i_{mea} and C^i_{calc} at each depth *i* were calculated using the mean square error (MSE) as:

$$MSE = \frac{1}{N}\sum_{i=1}^{N}\left(\frac{c^i_{mea} - c^i_{calc}}{c^i_{mea}}\right)^2 \qquad \text{(Eq. 3)}.$$

The minimized sum of the MSE for Fe^{2+}, HS^-, and $\delta^{56}Fe_{diss}$ was used to find the best fitting parameters. The respective constants k_2 applied for R2 were 0.2, 0.4, and 0.8. The best fit based on the minimum MSE was achieved with k_2=0.4 (Fig. 8). The reaction front of Fe_{diss} and HS^- varies with the value k_2. Although there is no isotopic Fe fractionation considered for reaction R2, the changed H_2S profile leads to a different depth for the reaction R3 and, thus, a different $\delta^{56}Fe_{diss}$ profile. The constants k_3 tested for R3 (in combination with k_2=0.4) were 2, 4, and 8. The H_2S concentration profile shows a higher dependency on R2 (or k_2) compared to R3 (or k_3). The best data fit resulted from applying k_3=4.

https://doi.org/10.5194/egusphere-2024-1942
Preprint. Discussion started: 17 July 2024
© Author(s) 2024. CC BY 4.0 License.

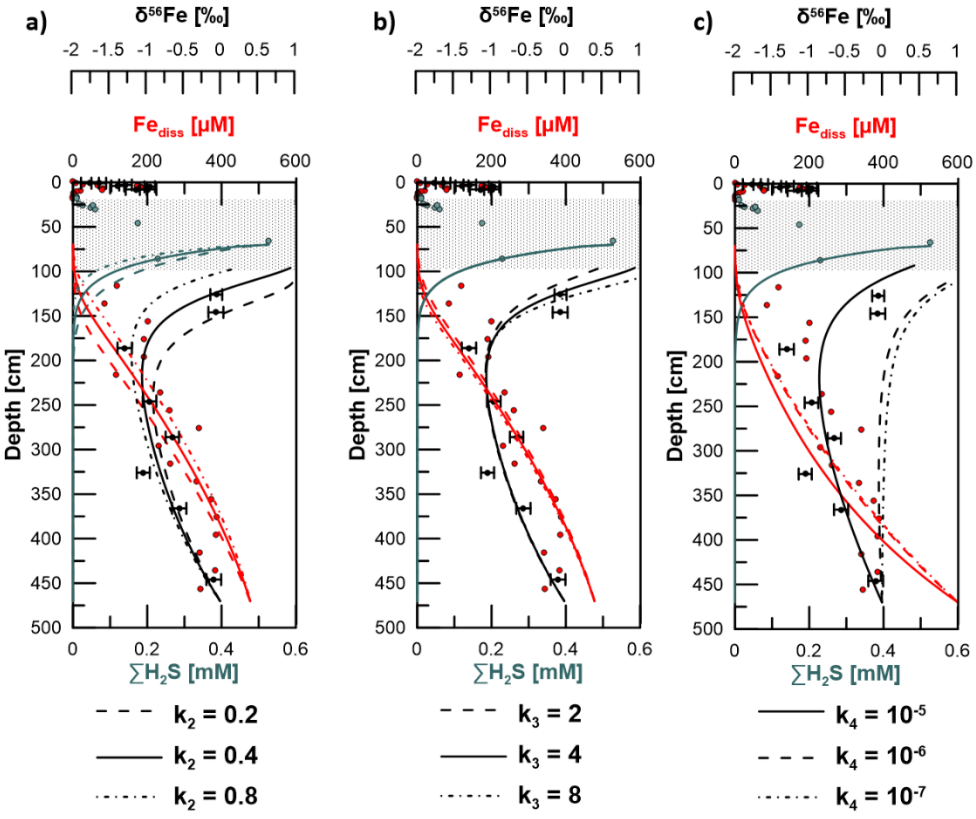

Figure 8: Sensitivity test by application of different reaction rate constants (k) for a) R2 (reaction of free hydrogen sulfide with solid Fe oxides), b) R3 (iron sulfide formation by reaction of Fe^{2+} with HS^-), and c) R4 (adsorption of Fe^{2+}). Solid lines represent the best fit to the measured data and were thus used in the model to determine kinetic fractionation factors (see Table S2). Uncertainty bars are 2SD.

Using k_2=0.4 and k_3=4 achieved for R2 and R3, the best fit of the modelled $\delta^{56}Fe_{diss}$ profiles with the respective measured data was achieved when setting the kinetic fractionation factor α_1 for MIR (DIR) (R1) to 0.997 and α_3 for sulfide precipitation via reaction of Fe^{2+} with HS^- (R3) to 0.998 (Fig. 9). As R1 is not confined to a narrow interval as it is the case for R3, the effect of the choice of α_1 on the overall $\delta^{56}Fe_{diss}$ profile is much stronger than the choice of α_3. The value chosen for α_3 is, of course, most relevant for the depth of ~100 cm, where HS^- formation occurs. Here, the choice of the fractionation factor results in differences of $\delta^{56}Fe_{diss}$ of more than 2‰ (Fig. 9; modelled profile with α_3=0.997 not shown completely due to limitation of x-axis to 1‰).

https://doi.org/10.5194/egusphere-2024-1942
Preprint. Discussion started: 17 July 2024
© Author(s) 2024. CC BY 4.0 License.

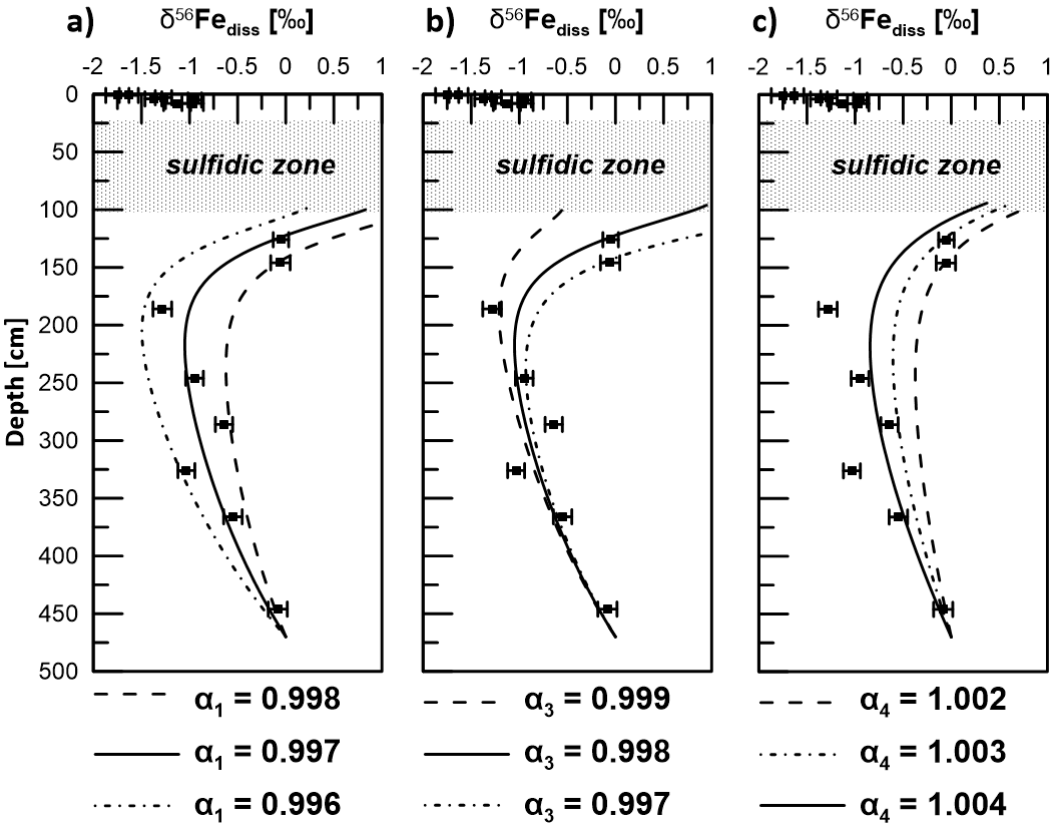

Figure 9: $\delta^{56}Fe_{diss}$ profiles derived by applying a transport-reaction model and different kinetic fractionation factors for a) Microbial iron reduction (α_1), b) pyrite formation via Fe^{2+} and HS^- counter-diffusion (α_3), and c) adsorption of Fe^{2+} (α_4). Solid lines represent the best fit to measured data (filled circles). Uncertainty bars are 2SD.

4 Discussion

4.1 Redox zones, reaction fronts and sediment composition

385 The kink shape of the sulfate profile indicates some bioturbation and/or bioirrigation in the top 15 cm of the sediment (e.g., Henkel et al., 2011; Fischer et al., 2012), which is conclusive with the general intense bioturbation at Site HE443/10 evidenced by the radiographs (xxx). However, this does not result in a high O_2 penetration depth as demonstrated by the presence of dissolved Mn (~35 µM) at 1 cm and the maximum concentration at 3 cm (Fig. 3). Manganese oxides are considered to get microbially reduced as soon as the pore water is depleted of more favourable electron acceptors such as O_2 and nitrate (e.g.,

https://doi.org/10.5194/egusphere-2024-1942
Preprint. Discussion started: 17 July 2024
© Author(s) 2024. CC BY 4.0 License.

Burdige, 1993). The Fe_{diss} profile (Fig. 2) is smooth and shows comparatively high concentrations of up to 180 µM at 5 cm depth. Therefore, we consider the direct effect of bioturbation/bioirrigation on pore water geochemistry to be minor. The Fe liberation in this interval is mainly due to MIR as has been described in detail in Henkel et al. (2016) for a site located ~100 m away from Site HE443/10.

The investigated sediments are rich in total and reactive Fe. The averages are 28 and 9 mg/g sediment, respectively (Fig. 4). The Fe/Al ratio is ~0.59, which is close to the average shale composition of 0.55 (Wedepohl, 1991). There is no downcore decrease of Fe_{total}, Fe/Al or the reactive/extractable Fe pool as seen for example in Thamdrup et al. (1994) in sediments of Aarhus Bay (Denmark) and Severmann et al. (2006) in deposits of the Santa Barbara Basin. In the case of constant accumulation rates and a consistent composition of the accumulated material, a decrease of Fe or reactive Fe phases with depth is indicative of microbial Fe reduction, upward Fe^{2+} diffusion, and Fe oxide precipitation at the redox boundary. The absence of such a decrease at site HE433/10 is likely due to intense reworking of the sediment. Bioturbation results in a very effective mixing of solid phases in the top few centimetres.

Under the assumption that the Fe/Al ratio of the detrital material transported to the HMA area has been constant over time, intervals with high Fe/Al ratios and Fe contents (e.g., 230-300 cm) reflect enrichments of Fe due to diagenetic Fe mineral formation. The intervals of lower Fe/Al and Fe_{total} contents in contrast rather indicate loss of Fe through early diagenetic Fe reduction and subsequent diffusion. However, Fe oxide dissolution and secondary mineral formation might have been blurred in the record if they happened while the sediment was still in the zone affected by bioturbation. The release of Fe_{diss} into the pore water, in particular at ~5 and 400 cm depth, and the presence of Fe monosulfides and pyrite in the whole sediment column generally reflect that Fe phases at site HE443/10 undergo considerable early diagenetic transformation. Iron sulfides are indicative for the reaction of solid Fe(III) or Fe^{2+} with hydrogen sulfide which is released during organoclastic of methane-mediated sulfate reduction (e.g., Poulton et al., 2004; Jørgensen and Kasten, 2006; Riedinger et al., 2017). The peak in H_2S indicates that sulfate-mediated AOM takes place at ~70 cm. There is a higher diffusive flux J_{sed} of HS^- (~ -13 mmol m^{-2} yr^{-1}) compared to Fe_{diss} (0.60 mmol m^{-2} yr^{-1}) towards the sulfidization front at 100 cm (Fig. 2). Consequently, there is not only precipitation as FeS, but also formation of pyrite from these monosulfides and Fe oxides: The removal of HS^- from pore water by sulfide formation or re-oxidation exceeds the removal of Fe_{diss}.

https://doi.org/10.5194/egusphere-2024-1942
Preprint. Discussion started: 17 July 2024
© Author(s) 2024. CC BY 4.0 License.

The most reactive Fe (oxyhydr)oxides with respect to H_2S are hydrous ferric oxides, ferrihydrite and lepidocrocite, followed by goethite, magnetite, and hematite (Findlay et al., 2020; Michaud et al. 2020; Poulton et al., 2004). The comparably high Fe_{hyam} contents at Site HE443/10 indicate that the amount of H_2S has never been high enough or the time the sediment was subjected to sulfidic conditions has never been long enough to lead to a complete transformation of the highly reactive Fe oxide pool into iron monosulfides or pyrite. The high Fe_{hyam} contents are at least partly attributed to lepidocrocite that has been detected earlier by Mössbauer spectroscopy in methanic sediments of the HMA (Oni et al., 2015a). It needs to be noted that recent incubation studies showed that the term "reactive" Fe oxides as we use it here based on chemical extraction is not necessarily identical to the fraction that is "biologically available" (Aromokeye et al., 2020; Wunder et al., 2024).

There is an enrichment of Fe sulfides (mostly CRS) within the current sulfidic zone and in particular at or close to the upper sulfurization front at 10 cm depth, where Fe_{diss} and H_2S react to FeS, which is subsequently transformed into pyrite (Fig. 4). This enrichment shows that despite the strong reworking of the sediment, the sulfidic zone must have been fixed to this interval for some years, which is consistent with the low sedimentation rates of <3 mm/yr during the past ~700 years. The above-mentioned Fe_{total} enrichment between 230 and 300 cm is not related to a CRS maximum, so it does not represent a paleo-SMT. It is rather attributed to the Fe_{aca} pool potentially indicating a diagenetic formation of Fe-carbonates (siderite) or AVS. (At Site HE443/10 siderite is oversaturated below 100 cm depth, see Fig. S1.) The Fe enrichment is also, to a lesser extent, reflected by Fe_{hyam} and $Fe_{di\text{-}ct}$ which indicates that this interval has either been "recharged" a lot with diagenetic Fe oxides by oxidation of the upward diffusing Fe^{2+} when this interval was close to the surface or that it was buried more rapidly than sediment above and below so that Fe oxides were not so much affected by pyritization. Since the interval does not show stronger signs of bioturbation than the rest of the core, which could favour a strong reoxidation of Fe^{2+} and FeS, and since sedimentation rates were high when this interval accumulated, we consider the faster burial through the sulfidic zone to be the more plausible explanation for the Fe enrichment observed between 230 and 300 cm.

The extraction wit sodium acetate targets Fe associated with carbonates (Poulton and Canfield, 2005; Tessier et al., 1979), but is known to also partly dissolve monosulfides etc. (AVS) (Cornwell and Morse, 1987; Poulton and Canfield, 2005) and surface-reduced Fe(II) (Crosby et al., 2005; 2007; Henkel et al., 2016). As we extracted AVS separately, we could attribute 6 to 26% of the Fe_{aca} pool in samples from Site HE443/10 to AVS. Particularly high contributions of AVS to Fe_{aca} are found at

https://doi.org/10.5194/egusphere-2024-1942
Preprint. Discussion started: 17 July 2024
© Author(s) 2024. CC BY 4.0 License.

116 cm just below the current depth of the lower sulfidization front, at 236 cm (depth of the above-mentioned Fe enrichment) and at 396 cm. The presence of AVS below the sulfidic zone is consistent with the findings of Riedinger et al. (2017) that metastable authigenic iron monosulfides can survive burial into deeper sediments in highly dynamic depositional systems, where high sedimentation rates and high Fe oxide contents limit the exposure to free HS^- restricted to a narrow zone around the SMT.

Diagenetic processes and reaction fronts in marine sediments are ultimately determined by the quality amount of accumulated TOC (e.g., Rullkötter 2006). In order to assess whether reaction fronts might have shifted up- or downwards in the past, in particular as a consequence of the above-mentioned decrease in sedimentation rates and a potential change in organic matter accumulation, we determined TOC contents. The preserved TOC contents at Site HE443/10 are all below 1.2 wt%. Considering some uncertainty as our study site is 5 km southwest of the core dated by Hebbeln et al. (2003) the shift in sedimentation rates should relate to a depth between 1 and 2 meters at HE433/10. Even though TOC values scatter between 0.4 and 1.2 wt%, there is no clear shift that would hint to this drastic change in depositional conditions. We conclude that the overall composition of material that was deposited in the HMA before and after ~700 yrs BP was similar and that the change was largely limited to the amount of material that was supplied. This is in line with previous observations by Oni et al. (2015b), who suggested similar sources of sediments and organic matter at and below the depth of the SMT based on low variation of $\delta^{13}C$ of TOC.

4.2 Iron isotope fractionation

As for other marine environments, where *in situ* Fe reduction in shallow sediments was observed (e.g., Henkel et al., 2016; 2018; Homoky et al., 2009; Severmann et al., 2006), there is, above the sulfidic zone, an overall downcore trend of $\delta^{56}Fe_{diss}$ towards heavier values (-1.75‰ at 1 cm vs. -1‰ at 8 cm). This trend is related to 1) the progressive removal of ^{54}Fe from the reducible ferric Fe pool during burial and ongoing MIR as well as to 2) progressive preferential removal of ^{54}Fe during interactions with hydrogen sulfide at the sulfidization front (Severmann et al., 2006). The availability of $^{54}Fe(III)$ is highest close to the oxic/anoxic boundary, which is reflected by most negative $\delta^{56}Fe_{diss}$ in the pore water. The processes above the sulfidic zone of HMA sediments were described earlier by Henkel et al. (2016). The easily reducible Fe(III) pool (Fe_{hyam}) contains Fe oxides that formed from isotopically light Fe_{diss} and is therefore also isotopically light compared to less reactive Fe oxide pools. This was already shown for shallow HMA sediments (Henkel et al., 2016), but can also be observed for the

https://doi.org/10.5194/egusphere-2024-1942
Preprint. Discussion started: 17 July 2024
© Author(s) 2024. CC BY 4.0 License.

deeper sediments investigated here ($\delta^{56}Fe_{hyam}$: -0.19 ± 0.16‰ (2SD) compared to $\delta^{56}Fe_{di\text{-}ct}$: 0.19 ± 0.08‰, $\delta^{56}Fe_{oxa}$: -0.09 ± 0.10‰).

Dissolved Fe concentrations measured right below the sulfidic zone, at ~130 cm, are ~100 µM. Respective $\delta^{56}Fe_{diss}$ values are ~0‰ (compared to -1.28‰ at ~190 cm, from where Fe is diffusing upwards). At first glance, this is in accordance with observations by Severmann et al. (2006) in sediments from Monterey Bay and Santa Barbara Basin and in sediments from Lake Kinneret (Sivan et al., 2011), where the formation of amorphous Fe sulfides drives $\delta^{56}Fe_{diss}$ towards positive values by preferential removal of ^{54}Fe from pore water. Experimental studies show that the $\delta^{56}Fe$ composition of FeS can be highly variable and depends on proportions of isotope exchange between particle and Fe_{diss} during aging of iron monosulfides (Guilbaud et al., 2010). Nevertheless, there is a general agreement that kinetic isotope fractionation, which dominates in natural sediments, leads to an isotopically light composition of amorphous Fe monosulfides compared to Fe_{diss} with $\Delta^{56}Fe_{FeS\text{-}Fe(II)diss}$ = -0.85 ± 0.30‰ ($\alpha_{FeS-Fe(II)diss}$= 0.999) (Butler et al., 2005; Roy et al., 2012). ^{54}Fe is further preferentially incorporated into pyrite (with FeS as precursor) as was shown by Guilbaud et al. (2011) for abiotic pyrite formation. Here, $\Delta^{56}Fe_{FeS2\text{-}FeS}$ is -1.70 to -3.0‰ ($\alpha_{FeS2-FeS}$ = 0.998 to 0.997), so the combined fractionation factor $\alpha_{FeS2-Fe(II)diss}$ (that can be compared to our α_3= 0.998, Fig. 9b) is 0.996 to 0.997. It needs to be considered that Fe sulfides age and exchange Fe isotopes with their surrounding (equilibrium fractionation). This is a process which takes place continuously in marine sediments. It might not be dominant, especially not at reaction fronts, but it causes a continuous equilibration of the Fe isotopic composition of different pools, also below the sulfidic interval.

At a second glance, however, it becomes apparent that there is a mismatch between the modelled Fe^{2+} and HS^- profile for this process at site HE443/10 and the respective measured data (Fig. 8b). From its source (AOM at ~70 cm depth) HS^- diffuses downwards and is used up already at a depth of ~120 cm, where Fe_{diss} is already at 118 µM. Based on the model output, HS^- would diffuse down to a depth of almost 150 cm and Fe_{diss} concentrations at ~130 cm would be close to zero. Furthermore, although we want to be cautious not to over-interpret a single datapoint, an Fe_{diss} sink is indicated by our measured pore-water profile at ~135 cm (loss of ~50% of the upward diffusing Fe). We conclude that siderite precipitation might occur at this specific interval. As for the precipitation of FeS, siderite formation would preferentially transfer ^{54}Fe into the solid phase ($\Delta^{56}Fe_{siderite\text{-}Fe(II)diss}$ = -0.48 ± 0.22‰, Wiesli et al., 2004). Unfortunately, the Fe_{aca} contents vary overall too much to resolve

https://doi.org/10.5194/egusphere-2024-1942
Preprint. Discussion started: 17 July 2024
© Author(s) 2024. CC BY 4.0 License.

where there is or has been a particular interval affected by siderite formation and $\delta^{56}Fe_{aca}$ in this potentially affected interval is similar to the $\delta^{56}Fe_{aca}$ directly above and below (Fig. 10). DIC concentrations are too high (>50 mM) to reflect a sink in the order of less than 2 mmol m^{-2} yr^{-1} as calculated from the loss of Fe_{diss} at 135 cm.

A Keeling plot (Fig. 6b) was used to determine the pore-water Fe isotope endmember for the observed deep Fe release. Here, we only used data from below those depths at which $\delta^{56}Fe_{diss}$ is mainly controlled by the reaction with H_2S, i.e., between 450 and 150 cm, where there is a rather linear $\delta^{56}Fe_{diss}$ trend (see Fig. S2 for reaction rates of R1-3). Although there is a linear trend between $1/[Fe_{diss}]$ and $\delta^{56}Fe_{diss}$ ($R^2 = 0.43$), the correlation is not statistically significant (p-value 0.161), which is partly due to the low amount of data points. The 95% confidence interval covers a wide range between -1.4 and +3.0‰ for the inferred Fe source (the intercept with the y-axis), it is not possible to determine the endmember without a large error. However, the Fe liberation at depth is most likely not causing a preferential release of ^{54}Fe. The lowermost $\delta^{56}Fe_{diss}$ value is -0.08 ± 0.10‰ and has thus an isotopic composition which is similar (within uncertainty) to the composition of Fe_{hyam} and Fe_{oxa} and is only slightly lighter than Fe_{dith} (Fig. 5).

The $\delta^{56}Fe_{diss}$ value at ~190 cm is -1.28 ± 0.10‰ (2SD), so while diffusing upwards, the Fe_{diss} either (1) loses ^{56}Fe or (2) is affected by an additional process providing ^{54}Fe. Removal of ^{56}Fe from pore water happens by preferential adsorption onto (Fe oxide) particles as has recently been shown by Köster et al. (2023). Over time, this Rayleigh distillation process progressively lowers $\delta^{56}Fe_{diss}$ values. Köster et al. (2023) used the fractionation factors $\Delta^{56}Fe_{Fe(II)sorb\text{-}Fe(II)diss}$=0.87‰ and 1.24‰ for adsorption of Fe(II) onto goethite surfaces (Beard et al., 2010; Crosby et al., 2007) to calculate the proportion of Fe_{diss} that would need to be "removed" (adsorbed) in order to obtain the extremely negative $\delta^{56}Fe_{diss}$ values that they measured in deep, lithified sediments from the Nankai Trough. Using the same approach here with $\delta^{56}Fe_{diss}$=0‰ for the deep Fe source, between 65 and 75% of the Fe_{diss} pool would need to get adsorbed to achieve a value of -1.28‰ at 190 cm. The Fe_{diss} concentration at ~190 cm is about 50% of $[Fe_{diss}]$ at 400 cm (Fig. 2). It is likely that adsorption (and also electron and atom exchange with different Fe minerals) takes place, which means that the concentration profile of Fe_{diss} in the methanic zone is not solely controlled by Fe_{diss} release at depth and Fe-S reactions as sink. Therefore, by implementing a reaction for adsorption based on Wang and Van Capellen (1996, see Table S1) and the rate expression $R_4 = -k_4[Fe^{2+}]$ with k_4 = 10^{-5}, 10^{-6} or 10^{-7} into our model, we tested if adsorption of Fe^{2+} plays a significant role (apart from being already included into the DIR fractionation factor α_1 as

https://doi.org/10.5194/egusphere-2024-1942
Preprint. Discussion started: 17 July 2024
© Author(s) 2024. CC BY 4.0 License.

515 described in section 2.5). k_4 includes the number of unoccupied surface sites, which is unknown. The test results do not produce a good fit between the modelled and measured Fe_{diss} profiles (Fig. 8c). Including α_4= 1.002, 1.003 or 1.004 for the respective preferential removal of the heavy isotope (in combination with k_4=10^{-5}) did also not lead to a good reproduction of the observed distinct shift of $\delta^{56}Fe_{diss}$ to -1.28‰ at ~190 cm (Fig. 9). Furthermore, the adsorbed (heavy) Fe should be transferred to the Fe_{aca} pool, but $\delta^{56}Fe_{aca}$ rather shows a trend towards more negative $\delta^{56}Fe_{aca}$ values with depth (Fig. 10). We conclude that adsorption
520 in the methanic sediments at site H433/10 is not the process dominating Fe removal from pore water and the trend towards lighter δ^{56}Fediss values between 450 and ~190 cm.

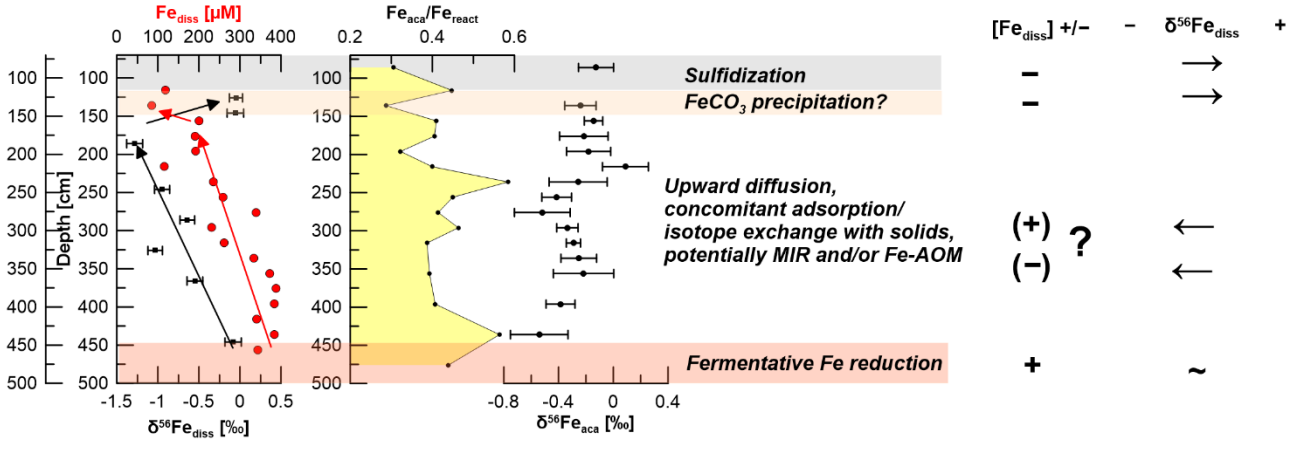

Figure 10: Interpretation of pore water and stable Fe isotopic data for site HE443/10: The deep Fe release does not go along with significant Fe fractionation and might be explained by fermentative processes. The red arrows show the overall trend of Fe_{diss}. The black arrows show the respective trends of $\delta^{56}Fe_{diss}$ values. The upward trend towards lighter isotopic values (between 450 and ~175 cm) might either be explained by low rates of microbial iron reduction (MIR), preferential removal of ^{56}Fe by adsorption or both. Additionally, Aromokeye et al. (2020) showed low rates of Fe-AOM in incubations of methanic HMA sediments. This process might also affect $\delta^{56}Fe_{diss}$. The shift towards positive $\delta^{56}Fe_{diss}$ values at ~150 cm likely indicates siderite precipitation.

Our PHREEQC calculations also indicate vivianite saturation in the methanic sediments. Vivianite is a ferrous iron phosphate
525 mineral, $Fe_3(PO_4)_2 \cdot 8\ H_2O$, which is known to be stable under anoxic sedimentary conditions, but its identification and quantification are difficult. Rothe et al. (2014) found that supersaturated pore water alone does not reliably predict vivianite

https://doi.org/10.5194/egusphere-2024-1942
Preprint. Discussion started: 17 July 2024
© Author(s) 2024. CC BY 4.0 License.

formation. Furthermore, there is no data available yet concerning the fractionation of iron during vivianite formation. Vuillemin et al. (2020) determined negative $\delta^{56}Fe$ values in vivianite crystals in more than 20 m deep sediments from Lake Towuti, Indonesia, but the dataset does not include pore-water data. We conclude that we have not enough data to assess the role of vivianite precipitation at our study site. However, vivianite formation would act as a phosphorous sink, and the PO_4 profile indicates a sink at ~300 cm. A slight shift in $\delta^{56}Fe_{diss}$ values towards negative values is recorded slightly below at 325 cm (Fig. 10). So, one could speculate that vivianite precipitation happens and preferentially incorporates ^{54}Fe.

For the model, we tested MIR as the factor controlling the trend of $\delta^{56}Fe_{diss}$ values towards -1.28‰ at between 450 cm and ~190 cm depth. We did so because MIR was stimulated in incubations of methanic sediments from this site when easily reducible Fe oxides (lepidocrocite) and benzoate were provided (Aromokeye et al., 2021). So, Fe reducing bacteria are present in these sediments, and Oni et al. (2015a) have also shown the presence of lepidocrocite. We also see a concurrent net Mn release in methanic sediments between 150 and 200 cm, but only at low levels, potentially because Mn solubility in non-sulfidic sediments is generally controlled by rhodocrosite or other mixed Mn/Ca carbonates (e.g., Gingele and Kasten, 1994). The net Mn release hints towards microbial metal reduction (overlap of MnO_2 reduction and MIR). In natural methanic sediments organoclastic DIR with fermentation intermediates such as acetate is generally assumed to not play an important role, because the related bacteria need acetate or other intermediates of fermentation products, which are typically not available at these depths. However, a recent study at a comparable site in Aarhus Bay (Kattegat) showed higher acetate concentrations below the SMT than above (Glombitza et al., 2019). Furthermore, through microbiological enrichment experiments, Aromokeye et al. (2021) demonstrated the potential that Fe liberation in the deeper sediments of the HMA is related to the activity of fermenting bacteria, and those are known to produce acetate (Lovely and Phillips, 1986). The OM in methanic sediments was previously characterized as recalcitrant O-rich aromatic and highly unsaturated compounds of terrestrial origin (Oni et al 2015b), but their methods could not resolve the distribution of low molecular weight compounds such as short chain fatty acids (including acetate). Microbes specialized in recalcitrant aromatic OM degradation often require an initial fermentation of the OM to fermentation intermediates (e.g., volatile fatty acids, reducing equivalents i.e., H_2 and acetate) that can be accessed by dissimilatory iron reducing organisms. In the methanic zone, fermentation intermediates such as acetate and H_2 are likely electron donors for methanogenesis whereas in surface sediments organic fermentation products are often

https://doi.org/10.5194/egusphere-2024-1942
Preprint. Discussion started: 17 July 2024
© Author(s) 2024. CC BY 4.0 License.

the electron donors for anaerobically respiring microorganisms with available electron acceptors (sulfate, iron oxides) (e.g., Beulig et al., 2018; Jørgensen, 2006; Whiticar, 1999; Yin et al., 2024). In our model, the applied MIR rate that produces a good fit to the measured $\delta^{56}Fe_{diss}$ data is very low (0.00011 mM yr^{-1}, Fig. S2) and does not explain Fe_{diss} concentrations of almost 400 µM at depth. When MIR rate takes place, the reactive ferric pool typically decreases with depth and becomes enriched in ^{56}Fe. The rate is, however, too low to reflect this in the solid phase data. The reactive Fe pool does not decrease with depth, and downcore isotopic trends are also absent for Fe_{hyam}, Fe_{dith}, and Fe_{oxa} (Fig. 4). We used a simple calculation to test how strongly the isotopic composition of the ferric Fe pool (here Fe_{hyam}) would change just by MIR at the rate applied in our model. The $\delta^{56}Fe_{hyam}$ at depth L can be calculated according to the mass balance equation,

$$\delta^{56}Fe^{0}_{hyam} \times Fe^{0}_{hyam} = \delta^{56}Fe^{L}_{hyam} \times Fe^{L}_{hyam} + (1-\alpha_1)\Delta Fe \quad \text{(Eq. 4)},$$

where Fe^{0}_{hyam} and Fe^{L}_{hyam} are the weight percent of Fe_{hyam} at the sediment surface and depth L (m), respectively, with its Fe isotope value $\delta^{56}Fe^{0}_{hyam}$ and $\delta^{56}Fe^{L}_{hyam}$. ΔFe is the amount of Fe that was lost due to Fe_{diss} release by MIR, i.e., $\Delta Fe = Fe^{0}_{hyam} - Fe^{L}_{hyam}$. With a sedimentation rate ω = 0.0016 m yr^{-1} and a MIR rate R_1 = 0.00011 mM yr^{-1}, ΔFe is

$$\Delta Fe = \frac{4R_1 L M_{Fe}\phi}{\rho_s(1-\phi)} \times 100 \quad \text{(Eq. 5)}$$

where M_{Fe} is the molecular weight of iron. According to this, the Fe_{hyam} pool would lose only 0.014 wt% (0.14 mg/g) between sediment surface and 5 m depth. The isotopic difference of Fe_{hyam} between surface and 5 m depth would be 0.1‰, which is in the range of our analytical uncertainty (2SD).

We note that Aromokeye et al. (2020) also demonstrated that Fe-AOM occurs at low rates, in particular right below the sulfidic zone. This process that releases 8 mol of Fe_{diss} for each mol of CH_4 might potentially also play a role. But as there is no literature data on respective Fe fractionation, our study cannot resolve whether it is solely MIR or MIR and Fe-AOM occurring at low rates (Fig. 10).

We observe that high Fe_{dith} contents are related to slightly higher $\delta^{56}Fe_{dith}$ values (Fig. 6a), a situation that is counter-intuitive assuming that ^{54}Fe would be preferentially lost when the Fe_{dith} pool would be reduced by microbes, so lower contents should go along with a more positive $\delta^{56}Fe_{dith}$ value. The Miller-Tans plot should therefore not be interpreted as reflecting downcore trends: Fe_{dith} (as well as Fe_{aca}, Fe_{hyam}, and Fe_{oxa}) maxima are recorded within the methanic interval (Fig. 4). The plot demonstrates that the isotopic differences between sequentially extracted Fe pools are largest (but still small) where Fe contents

https://doi.org/10.5194/egusphere-2024-1942
Preprint. Discussion started: 17 July 2024
© Author(s) 2024. CC BY 4.0 License.

are highest - a circumstance that is also unexpected since the isotopic fractionation in the (remaining) substrate should be expressed more strongly if the ferric Fe pool is small. Possibly, this is an effect of non-steady state conditions in the past. Overall, the Fe_{oxa} pool is not affected by Fe isotope fractionation, but all other extracted Fe(III) pools are. The pools that are known to contain sorbed Fe(II) and typical secondary minerals (Fe_{aca} and Fe_{hyam}) which form from (isotopically light) Fe_{diss}, and are therefore characterized by overall negative $\delta^{56}Fe$ values and, as expected, lighter composition at higher contents. Only the $\delta^{56}Fe_{dith}$ pool shows a slight shift towards positive values at higher contents, which we cannot entirely resolve here. Considering that the iron released at depth has an isotopic composition close to 0‰, adsorbed iron deriving from upward diffusion would potentially have a positive $\delta^{56}Fe$ signature. If part of the adsorbed (heavy) iron is then exchanged with the reactive Fe oxide surface (Crosby et al. 2007) and might subsequently even migrate deeper into the iron oxide crystal (Larese-Casanova et al., 2023), it could cause an alteration of Fe oxide isotope signatures towards positive values without reducing the mineral. It might also be speculated that adsorption and the related electron and atom exchange are more prevalent at depths that have a high Fe oxide (Fe_{dith}) content, but this interpretation remains very speculative, in particular because our model does not indicate adsorption to be a dominant Fe sink.

4.3 Deep iron release

Deep iron reduction can occur purely abiotically via oxidation of reduced sulfur compounds (e.g., Holmkvist et al., 2011; Riedinger et al., 2010). However, Fe reduction due to this so-called cryptic S cycling fails as an explanation for the build-up of Fe_{diss} far below the sulfidic zone, as has also been concluded by Riedinger et al. (2014) for Fe-rich continental margin sediments off Argentina, Egger et al. (2014) for Bothnian Sea sediments, and Oni et al. (2015a) for the methanic sediments of the HMA.

The correlation of Fe_{diss} concentrations with JS1 bacteria, methanogens, and *Methanohalobium*/ANME-3 related archaea at our study site suggested that the deep Fe reduction is coupled to the activity of these microbes (Oni et al. 2015a). An overlap of hydrogenotrophic CH_4 production and Fe-AOM has also been proposed based on the isotopic composition of CH_4 in sediments from the Baltic Sea (Egger et al. 2014; 2017). Several incubation experiments have demonstrated that the addition of reducible Fe oxides can stimulate Fe-AOM in natural sediments characterized by low/absent sulfate concentrations (Aromokeye et al. 2020; Beal et al., 2009; Egger et al., 2014; Segarra et al., 2013; Sivan et al., 2011). Aromokeye et al. (2020,

https://doi.org/10.5194/egusphere-2024-1942
Preprint. Discussion started: 17 July 2024
© Author(s) 2024. CC BY 4.0 License.

2021), however, found that in incubations of HMA sediment, Fe release occurred not entirely, but largely unrelated from methane oxidation and seemed to be rather linked to the fermentation of complex organic matter – a process that can be stimulated by crystalline Fe oxides because 1) fermenters reduce Fe(III) as an outlet for electrons primarily to overcome the thermodynamic barriers caused by high concentrations of newly produced fermentation intermediates, thus enabling continued degradation OM (fermentative iron reduction; Hopkins et al., 1995; Lovley, 1991) and 2) the conductive character of the Fe oxides facilitates interspecies electron transfer from fermenting bacteria towards methanogens (Kato et al. 2012; Lovley and Holmes, 2022).

Building on all these previous studies, our iron isotopic data further hint towards a deep Fe release that is not linked to DIR or another process in which microbes would preferentially use isotopically light Fe oxides. Fermenting bacteria typically require a syntrophic partner such as a H_2 utilizing bacteria (Hopkins et al, 1995) or a methanogen (e.g., Kato et al., 2012). The syntrophic partner consumes fermentation intermediates as a primary pathway for electron release and for thermodynamic feasibility of OM degradation. In the absence of a syntrophic partner, fermenting bacteria have been shown to be capable of electron transfer to iron oxides to further promote OM degradation. The iron oxides may be reduced fortuitously in the process as final sink for the electrons or serve as conduit further transferring the electrons to an available syntroph, e.g., a methanogen (Aromokeye et al, 2021). The fermenting bacteria that transfer electrons to crystalline Fe oxides do not directly profit from Fe(III) reduction beyond the removal of thermodynamic limitations brought about by accumulation of fermentation intermediates. In other words: The fermenters use the conductive Fe oxides to transfer electrons and to be able to continue with the fermentation of particularly aromatic OM. The transfer of electrons via conductive Fe oxides speeds up the degradation of aromatic compounds and is beneficial to both partner microbes (e.g., Jiang et al., 2013; Kato et al., 2012; Zhuang et al., 2015). Figure 11 summarizes how fermenting bacteria, MIR performing bacteria and methanogens are known to interact and how the deep iron release observed/found in the sediments of the HMA could be explained. Unfortunately, there are, to our knowledge, no studies available that show how fermentative iron reduction takes place mechanistically, i.e., directly or indirectly by the fermenting bacteria or during the interspecies electron transfer. Also, there are no experimental studies on how fermentative iron reduction fractionates iron isotopes. This is a gap of knowledge that should be addressed by future studies. In any case, the reason for the supposed fermentative Fe reduction happening at depth and not, e.g., directly below the

https://doi.org/10.5194/egusphere-2024-1942
Preprint. Discussion started: 17 July 2024
© Author(s) 2024. CC BY 4.0 License.

sulfidic zone might be selective OM degradation with more aromatic or unsaturated compounds in the deep sediment (Gibson and Harwood, 2002; Oni et al., 2015b).

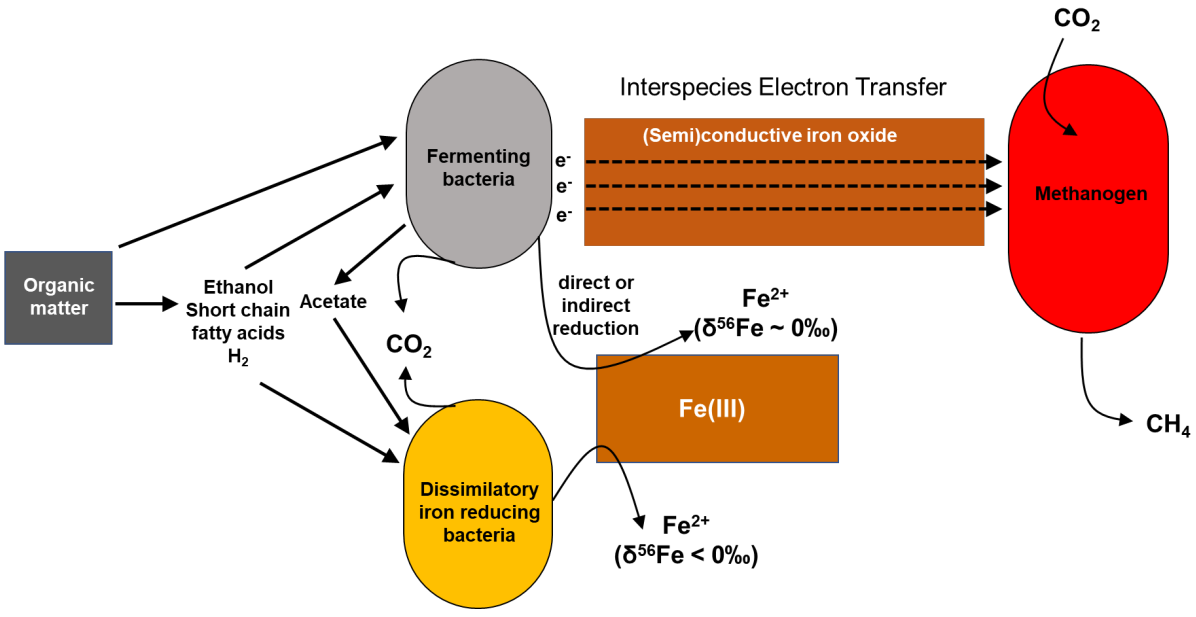

Figure 11: Schematic representation of how deep iron reduction in methanic sediments of the HMA could be controlled. The relative contributions of microbial iron reduction (here DIR) and fermentative iron reduction likely depend on the availability of Fe oxides, the composition of the organic matter and the abundance of methanogens as "partner organisms" to which fermenters transfer electrons.

4.4 Applicability of iron isotopes to trace iron processes in marine sediments

We demonstrate that the application of iron isotopes in marine sediments provides information that helps identifying or verifying specific Fe reaction pathways. However, the main difficulty in using iron isotopes in natural systems is that usually, various processes of Fe liberation and incorporation into solid phases are at play simultaneously. In the deep HMA sediments which contain lepidocrocite (Oni et al. 2015a) as well as crystalline Fe oxides, different pathways of microbial organic matter oxidation with involvement of Fe-phases are likely to happen simultaneously – namely microbial iron reduction and fermentative processes with electron shuttling. These processes are therefore hard to resolve by iron isotope data alone.

https://doi.org/10.5194/egusphere-2024-1942
Preprint. Discussion started: 17 July 2024
© Author(s) 2024. CC BY 4.0 License.

Generally, when multiple iron reactions are taking place, the resulting Fe isotope signals in dissolved and solid pools might not reflect or resolve all specific fractionation processes. Furthermore, over time, equilibrium isotope fractionation overprints kinetic isotope fractionation, so the isotopic composition of two pools that are susceptible to atom exchange, will change until heavy isotopes are enriched in the pool with "stiffer" bonds (e.g., Wiederhold et al., 2015). We also note potential challenges when working with sequentially extracted Fe pools. As has been shown previously, these pools are not mineral specific (e.g., Henkel et al., 2016). If the overall content of a pool is large compared to the amount of Fe in that pool that was affected by diagenesis, then the respective isotopic differences (e.g., downcore) might still be in the range of the analytical uncertainty. So, depending on the setting, resolving differently reactive Fe phases and analysing the respective δ^{56}Fe signals, might not be specific enough to clearly deduce which processes take place. This study and the comparison to the study of Köster et al. (2023) demonstrate that, unsurprisingly, processes dominating the shape of δ^{56}Fe profiles and records differ depending on depth for two reasons: 1) The microbial community changes in composition and quantity due to depth-dependent availabilities of organic matter and electron acceptors and 2) equilibrium fractionation and processes like adsorption become increasingly important with the age of the studied sediment. In any case, the application of Fe isotopes in marine sediments requires a large set of complementary geochemical and microbiological data to achieve a robust interpretation.

5 Summary and conclusions

Here we applied stable iron isotope analyses on pore water and sequentially extracted, differently reactive iron phases and transport/reaction modelling to identify the process responsible for the observed deep iron release in methanic sediments of the Helgoland mud area. The comparison between the isotopic composition of dissolved Fe and the ferric solid substrates reveals that the deep Fe release is not leading to a preferential liberation of ^{54}Fe as it occurs during DIR in shallow sediments. In combination with previous microbial studies, this isotopic study implies that iron reduction occurs during fermentative iron reduction when electrons are transferred from fermenters to iron oxides. In contrast to DIR, the "choice" of iron isotopes during the reduction seems to be rather coincidental. However, studies on the mechanistic details of fermentative iron reduction (including Fe isotope analyses) are needed to proof our interpretation.

https://doi.org/10.5194/egusphere-2024-1942
Preprint. Discussion started: 17 July 2024
© Author(s) 2024. CC BY 4.0 License.

This study provides a concept on how to deal with the complexity of geochemical and in particular Fe isotope data from pore water and sediments in order to test whether specific Fe redox reactions are or aren't at play. We conclude that in combination with microbial experiments and geochemical and transport/reaction modelling, basic additional knowledge about Fe reactions can be gained by applying Fe isotope geochemistry. However, data interpretation is still far from being straight-forward. This study also demonstrates that a robust data interpretation relies on the combination of methods and the involvement of different expertise.

Data availability

Data are available at https://doi.org/10.1594/PANGAEA.893760, https://doi.org/10.1594/PANGAEA.893766 (Aromokeye et al.; 2020) and xxx [will be included, uploaded to PANGAEA, but no doi yet].

Author contribution

SH and SK have designed the study. MS, AM and SAK have provided expertise, access to MC-ICPMS instruments and technical support. BL performed the modelling. SH has compiled the geochemical data and wrote the manuscript with contributions from all co-authors. All co-authors were involved in data discussion.

Competing interests

The authors declare that they have no conflict of interest.

Acknowledgments

We thank Ingrid Stimac (AWI), Ingrid Dohrmann (AWI), Jochen Scheld (University of Cologne), and Johann Hollop (at that time student at the University of Bremen) for their support during sample processing. We particularly thank Clara Sena, who provided the thermodynamic database used in the PHREEQC calculations as well as the sample input files. Gerhard Kuhn (AWI) is thanked for providing TOC and TC data.

https://doi.org/10.5194/egusphere-2024-1942
Preprint. Discussion started: 17 July 2024
© Author(s) 2024. CC BY 4.0 License.

Funding: This work was funded by the ResearchCenter/Cluster of Excellence "The Ocean Floor – Earth's Uncharted Interface" and the MARUM – Center for Marine Environmental Sciences, University of Bremen. Bo Liu received financial support from the BMBF-funded MARE:N project "Anthropogenic impacts on particulate organic carbon cycling in the North Sea (APOC)" (grant no. 03F0874A). We acknowledge further financial support from the Helmholtz Association (Alfred Wegener Institute Helmholtz Centre for Polar and Marine Research).

References

Arndt, S., Jørgensen, B. B., LaRowe, D. E., Middelburg, J. J., Pancost, R. D., and Regnier, P.: Quantifying the degradation of organic matter in marine sediments: A review and synthesis, Earth Sci. Rev., 123, 53-86, doi: 10.1016/j.earscirev.2013.02.008, 2013.

Aromokeye, D. A., Kulkarni, A., Elvert, M., Wegener, G., Henkel, S., Coffinet, S., Eickhorst, T., Oni, O. E., Richter-Heitmann, T., Schnakenberg, A., Taubner, H., Wunder, L., Yin, X., Zhu, Q., Hinrichs, K.-U., Kasten, S., and Friedrich, M. W.: Rates and microbial players of iron-driven anaerobic oxidation of methane in methanic marine sediments, Front. Microbiol., 10, 3041, doi: 10.3389/fmicb.2019.03041, 2020.

Aromokeye, D. A., Oni, O. E., Tebben, J., Yin, X., Richter-Heitmann, T., Wendt, J., Nimzyk, R., Littmann, S., Tienken, D., Kulkarni, A. C., Henkel, S., Hinrichs, K.-U., Elvert, M., Harder, T., Kasten, S., and Friedrich M. W.: Crystalline iron oxides stimulate methanogenic benzoate degradation in marine sediment-derived enrichment cultures, ISME J, 15, 965–980, doi: 10.1038/s41396-020-00824-7, 2021.

Baloza, M., Henkel, S., Geibert, W., Kasten, S., and Holtappels, M.: Benthic carbon remineralization and iron cycling in relation to sea ice cover along the eastern continental shelf of the Antarctic Peninsula, JGR Oceans, 127, 7, e2021JC018401, doi: 10.1029/2021JC018401, 2022.

Bao, P. and Li, G. X.: Sulfur-driven iron reduction coupled to anaerobic ammonium oxidation, Environ. Sci. Technol., 51, 6691-6698, doi: 10.1021/acs.est.6b05971, 2017.

Beal, E. J., House, C. H., and Orphan, V. J.: Manganese- and iron-dependant marine methane oxidation, Science, 325,184-187, doi: 10.1126/science.1169984, 2009.

Beard, B. L., Johnson, C. M., Cox, L., Sun, H., Nealson, K. H., and Aguliar, C.: Iron isotope biosignatures, Science, 285, 1889-1892, doi: 10.1126/science.285.5435.1889, 1999.

Beard, B. L., Johnson, C. M., Skulan, J. L., Nealson, K. H., Cox, L., and Sun, H.: Application of Fe isotopes to tracing the geochemical and biological cycling of Fe, Chem. Geol., 195, 87–117, doi: 10.1016/S0009-2541(02)00390-X, 2003a.

Beard, B. L., Johnson, C. M., Von Damm, K. L., and Poulson, R. L.: Iron isotope constraints on Fe cycling and mass balance in the oxygenated Earth oceans, Geology, 31, 629–632, doi: 10.1130/0091-7613(2003)031<0629:IICOFC>2.0.CO;2, 2003b.

https://doi.org/10.5194/egusphere-2024-1942
Preprint. Discussion started: 17 July 2024
© Author(s) 2024. CC BY 4.0 License.

Beard, B. L., Handler, R. M., Scherer, M. M., Wu, L., Czaja, A. D., Heimann, A., and Johnson C. M.: Iron isotope fractionation between aqueous ferrous iron and goethite, EPSL, 295, 241-250, doi: 10.1016/j.epsl.2010.04.006, 2010.

Beulig, F., Røy, H., Glombitza, C., and Jørgensen, B. B.: Control on rate and pathway of anaerobic organic carbon degradation in the seabed, Proc. Natl. Acad. Sci., 115, 367–372, doi: 10.1073/pnas.1715789115, 2018.

Bottrell, S. H., Parkes, R. J., Cragg, B. A., and Raiswell, R.: Isotopic evidence for anoxic pyrite oxidation and stimulation of bacterial sulphate reduction in marine sediments, J. Geol. Soc., 157, 711-714, doi: 10.1144/jgs.157.4.711,2010.

Boudreau, B. P.: The diffusive tortuosity of fine-grained unlithified sediments. Geochim. Cosmochim. Acta, 60, 3139-3142, doi: 10.1016/0016-7037(96)00158-5, 1996.

Boudreau, B. P.: Diagenetic models and their implementation: Modelling transport and reactions in aquatic sediments, Springer, doi: 10.1007/978-3-642-60421-8, 1997.

Burdige, D. J.: The biogeochemistry of manganese and iron reduction in marine sediments, Earth Sci. Rev., 35(3), 249–284, doi: 10.1016/0012-8252(93)90040-E, 1993.

Butler, I. B., Archer, C., Vance, D., Oldroyd, A., and Rickard, D.: Fe isotope fractionation on FeS formation in ambient aqueous solution, EPSL 236, 430-442, doi: 10.1016/j.epsl.2005.05.022, 2005.

Canfield, D. E., Raiswell, R., Westrich, J. T., Reaves, C. M., and Berner, R. A.: The use of chromium reduction in the analysis of reduced inorganic sulfur in sediments and shales, Chem. Geol. 54, 149–155, doi: 10.1016/0009-2541(86)90078-1, 1986.

Canfield, D. E.: Reactive iron in marine sediments, Geochim. Cosmochim. Acta, 53, 619-632, doi: 10.1016/0016-7037(89)90005-7,1989.

Cline, J. D.: Spectrophotometric determination of hydrogen sulfide in natural waters, Limnology and Oceanography, 14, 454-458, doi: 10.4319/lo.1969.14.3.0454, 1969.

Conway, T. M. and John, S. G.: Quantification of dissolved iron sources to the North Atlantic Ocean, Nature, 511, 212-215, doi: 10.1038/nature13482, 2014.

Cornwell, J. C. and Morse, J. W.: The characterization of iron sulfide minerals in anoxic marine sediments. Mar. Chem., 22, 193– 206, doi: 10.1016/0304-4203(87)90008-9, 1987.

Crosby, H. A., Johnson, C. M., Roden, E. E., and Beard B. L.: Coupled Fe(II)-Fe(III) electron and atom exchange as a mechanism for Fe isotope fractionation during dissimilatory iron oxide reduction, Environ. Sci. Technol., 39, 6698-6704, doi: 10.1021/es0505346, 2005.

Crosby, H. A., Roden, E. E., Johnson, C. M., and Beard, B. L.: The mechanism of iron isotope fractionation produced during dissimilatory Fe(III) reduction by *Shewanella putrefaciens* and *Geobacter sulfurreducens*, Geobiology, 5, 169–189, doi: 10.1111/j.1472-4669.2007.00103.x, 2007.

D'Hondt, S., Jørgensen, B. B., Miller, D. J., Batzke, A., Blake, R., Cragg, B. A., Cypionka, H., Dickens, G. R., Ferdelman, T., Hinrichs, K.-U., Holm, N. G., Mitterer, R., Spivack, A., Wang, G., Bekins, B., Engelen, B., Ford, K., Gettemy, G., Rutherford, S. D., Sass, H., Skilbeck, C. G., Aiello, I. W., Guèrin, G., House, C. H., Inagaki, F., Meister, P., Naehr, T., Niitsuma, S., Parkes,

https://doi.org/10.5194/egusphere-2024-1942
Preprint. Discussion started: 17 July 2024
© Author(s) 2024. CC BY 4.0 License.

R. J., Schippers, A., Smith, D. C., Teske, A., Wiegel, J., Padilla, C. N., and Acosta, J. L. S.: Distributions of microbial activities in deep subseafloor sediments, Science, 306, 2216-2221, doi: 10.1126/science.1101155, 2004.

Egger, M., Rasigraf, O., Sapart, C. J., Jilbert, T., Jetten, M. S., Rockmann, T., van der Veen, C., Banda, N., Kartal, B., Ettwig, K. F., and Slomp, C. P.: Iron-mediated anaerobic oxidation of methane in brackish coastal sediments, Environ. Sci. Technol., 49, 277-283, doi: 10.1021/es503663z, 2014.

Egger, M., Hagens, M., Sapart, C. J., Dijkstra, N., van Helmond, N. A. G. M., Mogollón, J. M., Risgaard-Petersen, N., van der Veen, C., Kasten, S., Riedinger, N., Böttcher, M. E., Rockmann, T., Jørgensen, B. B., and Slomp, C. P.: Iron oxide reduction in methane-rich deep Baltic Sea sediments, Geochim. Cosmochim. Acta, 207, 256-276, doi: 10.1016/j.gca.2017.03.019, 2017.

Eliani-Russak, E., Tik, Z., Uzi-Gavrilov, S., Meijler, M. M., and Sivan, O.: The reduction of environmentally abundant iron oxides by the methanogen *Methanosarcina barkeri*, Front. Microbiol., 14, 1197299, doi: 10.3389/fmicb.2023.1197299, 2023.

Findlay A., Pellerin A., Laufer K., and Jørgensen B.B.: Quantification of sulphide oxidation rates in marine sediments, Geochim. Cosmochim. Acta, 280, 441–452, 2020.

Fischer, D., Sahling, H., Nöthen, K., Bohrmann, G., Zabel, M., and Kasten, S.: Interaction between hydrocarbon seepage, chemosynthetic communities, and bottom water redox at cold seeps of the Makran accretionary prism: insights from habitat-specific pore water sampling and modelling, BG, 9, 2013–2031, doi: 10.5194/bg-9-2013-2012, 2012.

Gibson, J. and Harwood, S. C.: Metabolic diversity in aromatic compound utilization by anaerobic microbes, Annu. Rev. Microbiol., 56, 345-369, doi: 10.1146/annurev.micro.56.012302.160749, 2012.

Gingele, F. X. and Kasten, S.: Solid-phase manganese in Southeast Atlantic sediments: Implications for the paleoenvironment, Mar. Geol., 121:3–4, 317-332, doi: 10.1016/0025-3227(94)90037-X, 1994.

Glombitza, C., Egger, M., Røy, H., and Jørgensen, B. B.: Controls on volatile fatty acid concentrations in marine sediments (Baltic Sea), Geochim. Cosmochim. Acta, 258, 226–241, doi: 10.1016/j.gca.2019.05.038, 2019.

Guilbaud, R., Butler, I. B., Ellam, R. M., and Rickard, D.: Fe isotope exchange between $Fe(II)_{aq}$ and nanoparticulate mackinawite (FeS_m) during nanoparticle growth, EPSL, 300, 174-183, doi: 10.1016/j.epsl.2010.10.004, 2010.

Guilbaud, R., Butler, I. B., and Ellam, R. M.: Abiotic pyrite formation produces a large Fe isotope fractionation, Science, 332, 1548-1551, doi: 10.1126/science.1202924, 2011.

Henkel, S., Strasser, M., Schwenk, T., Hanebuth, T. J. J., Hüsener, J., Arnold, G. L., Winkelmann, D., Formolo, M., Tomasini, J., Krastel, S., and Kasten, S.: An interdisciplinary investigation of a recent submarine mass transport deposit at the continental margin off Uruguay, Geochem. Geophys. Geosys., 12:8, Q08009, doi: 10.1029/2011GC003669, 2011.

Henkel, S., Kasten, S., Poulton, S. W., and Staubwasser, M.: Determination of the stable iron isotopic composition of sequentially leached iron phases in marine sediments, Chem. Geol., 421, 93–102, doi: 10.1016/j.chemgeo.2015.12.003, 2016.

Henkel, S., Kasten, S., Hartmann, J. F., Silva-Busso, A., and Staubwasser, M.: Iron cycling and stable Fe isotope fractionation in Antarctic shelf sediments, King George Island, Geochim. Cosmochim. Acta, 237, 320-338, doi: 10.1016/j.gca.2018.06.042, 2018.

https://doi.org/10.5194/egusphere-2024-1942
Preprint. Discussion started: 17 July 2024
© Author(s) 2024. CC BY 4.0 License.

780 Hensen, C., Zabel, M., Pfeifer, K., Schwenk, T., Kasten, S., Riedinger, N., Schulz, H. D., and Boetius, A.: Control of sulfate pore-water profiles by sedimentary events and the significance of anaerobic oxidation of methane for the burial of sulfur in marine sediments, Geochim. Cosmochim. Acta, 67:14, 2631–2647, doi: 10.1016/S0016-7037(03)00199-6, 2003.

Hertweck, G.: Das Schlickgebiet in der inneren Deutschen Bucht. Aufnahme mit dem Sedimentechographen, Senckenbergiana marit., 15, 219–249, 1983.

785 Heuer, V. B., Inagaki, F., Morono, Y., Kubo, Y., Maeda, L., Bowden, S., Cramm, M., Henkel, S., Hirose, T., Homola, K., Hoshino, T., Ijiri, A., Imachi, H., Kamiya, N., Kaneko, M., Lagostina, L., Manners, H., McClelland, H. L., Metcalfe, K., Okutsu, N., Pan, D., Raudsepp, M. J., Sauvage, J., Schubotz, F., Spivack, A., Tonai, S., Treude, T., Tsang, M. Y., Viehweger, B., Wang, D. T., Whitaker, E., Yamamoto, Y., Yang, K., and Kinoshita, M.: Expedition 370 Preliminary Report: Temperature Limit of the Deep Biosphere off Muroto, International Ocean Discovery Program, doi: 10.14379/iodp.pr.370.2017, 2017.

790 Holmkvist, L., Ferdelman, T. G., and Jørgensen, B. B.: A cryptic sulfur cycle driven by iron in the methane zone of marine sediment (Aarhus Bay, Denmark), Geochim. Cosmochim. Acta, 75, 3581-3599, doi: 10.1016/j.gca.2011.03.033, 2011.

Homoky, W. B., Severmann, S., Mills, R. A., Statham, P. J., and Fones, G. R.: Pore-fluid Fe isotopes reflect the extent of benthic Fe redox recycling: Evidence from continental shelf and deep-sea sediments, Geology, 37(8), 751–754, doi: 10.1130/G25731A.1, 2009.

795 Hopkins, B. T., McInerney, M. J., and Warikoo, V.: Evidence for anaerobic syntrophic benzoate degradation threshold and isolation of the syntrophic benzoate degrader, Appl. Environ. Microbiol., 61:526, doi: 10.1128/aem.61.2.526-530.1995, 1995.

Ionescu, D., Heim, C., Polerecky, L., Thiel, V., and De Beer, D.: Biotic and abiotic oxidation and reduction of iron at circumneutral pH are inseparable processes under natural conditions, Geomicrobiol. J., 32:3-4, 221-230, doi: 10.1080/01490451.2014.887393, 2015.

800 Irion, G., Wunderlich, F., and Schwedhelm, E.: Transport of clay-minerals and anthropogenic compounds into the German Bight and the provenance of fine-grained sediments SE of Helgoland, J. Geol. Soc. London, 144, 153-160, doi: 10.1144/gsjgs.144.1.0153, 1987.

Jiang, S., Park, S., Yoon, Y., Lee, J.-H., Wu, M.-W., Phuoc, Dan N., Sadowsky, M. J., and Hur, H.-G.: Methanogenesis facilitated by geobiochemical iron cycle in a novel syntrophic methanogenic microbial community, Environ. Sci. Technol.,

805 47, 10078-10084, doi: 10.1021/es402412c, 2013.

Johnson, C. M. and Beard B. L.: Biogeochemical cycling of iron isotopes, Science, 309, 1025-1027, doi: 10.1126/science.1112552, 2005.

Johnson, C. M., Beard, B. L., Roden, E. E., Newman, D. K., and Nealson, K. H.: Isotopic constraints on biogeochemical cycling of Fe, Rev. Mineral. Geochem., 55, 359–408, doi: 10.2138/gsrmg.55.1.359, 2004.

810 Johnson, C. M., Roden, E. E., Welch, S. A., and Beard, B. L.: Experimental constraints on Fe isotope fractionation during magnetite and Fe carbonate formation coupled to dissimilatory hydrous ferric oxide reduction, Geochim. Cosmochim. Acta, 69, 963-993, doi: 10.1016/j.gca.2004.06.043, 2005.

https://doi.org/10.5194/egusphere-2024-1942
Preprint. Discussion started: 17 July 2024
© Author(s) 2024. CC BY 4.0 License.

Jørgensen, B. B.: Bacteria and Marine Biogeochemistry. In Marine Geochemistry. Schulz, H.D., and Zabel, M. (eds). Berlin, Heidelberg: Springer Berlin Heidelberg, pp. 169- 206, doi: 10.1007/978-3-662-04242-7_5, 2006.

Jørgensen, B. B. and Kasten, S.: Sulfur cycling and methane oxidation. In Marine Geochemistry, eds Schulz H.D. and Zabel M., Heidelberg, Springer-Verlag, 574, doi: 10.1007/3-540-32144-6_8, 2006.

Kasten, S., Freudenthal, T., Gingele, F. X., and Schulz, H. D.: Simultaneous formation of iron-rich layers at different redox boundaries in sediments of the Amazon deep-sea fan, Geochim. Cosmochim. Acta, 62:13, 2253–2264, doi: 10.1016/S0016-7037(98)00093-3, 1998.

Kato, S., Hashimoto, K., and Watanabe, K.: Methanogenesis facilitated by electric syntrophy via (semi) conductive iron-oxide minerals, Environ. Microbiol., 14, 1646-1654, doi: 10.1111/j.1462-2920.2011.02611.x, 2012.

Keeling, C. D.: The concentration and isotopic abundances of atmospheric carbon dioxide in rural areas, Geochim. Cosmochim. Acta, 13, 322–334, doi: 10.1016/0016-7037(58)90033-4, 1958.

Kerouel, R. and Aminot, A.: Fluorimetric determination of ammonia in sea and estuarine waters by direct segmented flow analysis, Mar. Chem., 57, 3-4, 265-275, doi: 10.1016/S0304-4203(97)00040-6, 1997.

Köster, M., Staubwasser, M., Meixner, A., Kasemann, S. A., Manners, H. R., Morono, Y., Inagaki, F., Heuer, V. B., Kasten, S., and Henkel, S.: Uniquely low stable iron isotopic signatures in deep marine sediments caused by Rayleigh distillation, Sci. Rep., 13, 10281, doi: 10.1038/s41598-023-37254-2, 2023.

Larese-Casanova, P., Yue, P., and Gorski, C.: Fe and O atom exchange on hematite and goethite surfaces after aqueous Fe(II) sorption: A NanoSIMS investigation, Goldschmidt 2023 Abstract, doi: 10.7185/gold2023.16329, 2023.

LaRowe, D. E. and P., Van Capellen: Degradation of natural organic matter: A thermodynamic analysis, Geochim. Cosmochim. Acta, 75, 2030-2042, doi: 10.1016/j.gca.2011.01.020, 2011.

Lehours, A. C., Rabiet, M., Morel-Desrosiers, N., Morel, J.-P., Jouve, L., Arbeille, B., Mailhot, G., and Fonty, G.: Ferric iron reduction by fermentative strain BS2 isolated from an iron-rich anoxic environment (Lake Pavin, France), Geomicrobiol. J., 27, 714-722, doi: 10.1080/01490451003597663, 2010.

Lovley, D. R.: Dissimilatory Fe(III) and Mn(IV) reduction, Microbiol. Rev., 55, 259-287, doi: 10.1016/S0065-2911(04)49005-5, 1991.

Lovley, D. R. and Holmes, D. E.: Electromicrobiology: the ecophysiology of phylogenetically diverse electroactive microorganisms, Nat. Rev. Microbiol., 20, 6-19, doi: 10.1038/s41579-021-00597-6, 2022.

Lovley, D. R. and Phillips, E. J.: Organic matter mineralization with reduction of ferric iron in anaerobic sediments, Appl. Environ. Microbiol., 51, 683-689, doi: 10.1128/aem.51.4.683-689.1986,1986.

Lovley, D. R., Phillips, E. J. P., and Lonergan, D. J.: Hydrogen and formate oxidation coupled to dissimilatory reduction of iron or manganese by *Alteromonas-putrefaciens*, Appl. Environ. Microb., 55, 700-706, doi: 10.1128/aem.55.3.700-706.1989, 1989.

https://doi.org/10.5194/egusphere-2024-1942
Preprint. Discussion started: 17 July 2024
© Author(s) 2024. CC BY 4.0 License.

März, C., Hoffmann, J., Bleil, U., De Lange, G. J., and Kasten, S.: Diagenetic changes of magnetic and geochemical signals by anaerobic methane oxidation in sediments of the Zambezi deep-sea fan (SW Indian Ocean), Mar. Geol., 255:3–4, 118-130, doi: 10.1016/j.margeo.2008.05.013, 2008.

Michaud, A. B., Laufer, K., Findlay, A., Pellerin, A., Antler, G., Turchyn, A. V., Røy, H., Wehrmann, L. M., and Jørgensen, B. B.: Glacial influence on the iron and sulfur cycles in Arctic fjord sediments (Svalbard), Geochim. Cosmochim. Acta, 280, 423–440, doi: 10.1016/j.gca.2019.12.033, 2020.

Miller, J. B. and Tans, P. P.: Calculating isotopic fractionation from atmospheric measurements at various scales, Tellus Ser B Chem. Phys. Meteorol., 55, 207–214, doi: 10.1034/j.1600-0889.2003.00020.x, 2003.

Mortimer, R. J. G., Galsworthy, A. M. J., Bottrell, S. H., Wilmot, L. E., and Newton, R. J.: Experimental evidence for rapid biotic and abiotic reduction of Fe (III) at low temperatures in salt marsh sediments: a possible mechanism for formation of modern sedimentary siderite concretions. Sedimentology, 58, 1514–1529, doi: 10.1111/j.1365-3091.2011.01224.x, 2011.

Oni, O., Miyatake, T., Kasten, S., Richter-Heitmann, T., Fischer, D., Wagenknecht, L., Kulkarni, A., Blumers, M., Shylin, S. I., Ksenofontov, V., Costa, B. F. O., Klingelhöfer, G., and Friedrich, M. W.: Distinct microbial populations are tightly linked to the profile of dissolved iron in the methanic sediments of the Helgoland mud area, North Sea, Front. Microbiol., 6:365, doi: 10.3389/fmicb.2015.00365, 2015a.

Oni, E. O., Schmidt, F., Miyatake, T., Kasten, S., Witt, M., Hinrichs, K.-U., and Friedrich, M.: Microbial communities and organic matter composition in surface and subsurface sediments of the Helgoland mud area, North Sea, Front. Microbiol., 6:1290, doi: 10.3389/fmicb.2015.01290, 2015b.

Parkhurst, D. L. and Appelo, C. A. J.: Description of input and examples for PHREEQC version 3 – a computer program for speciation, batch-reaction, one-dimensional transport, and inverse geochemical calculations, In: U.S. Geological Survey Techniques and Methods, 6 (497 p), 2013.

Pataki, D. E., Ehleringer, J. R., Flanagan, L. B., Yakir, D., Bowling, D. R., Still, C. J., Buchmann N., Kaplan, J. O., and Berry J. A.: The application and interpretation of Keeling plots in terrestrial carbon cycle research, Global Biogeochem. Cycles, 17, 1–14, doi: 10.1029/2001GB001850, 2013.

Poulton, S. W., Krom, M. D., and Raiswell, R.: A revised scheme for the reactivity of iron (oxyhydr)oxides towards dissolved sulfide, Geochim. Cosmochim. Acta, 68, 3703-3715, doi: 10.1016/j.gca.2004.03.012, 2004.

Poulton, S. W. and Canfield, D. E.: Development of a sequential extraction procedure for iron: implications for iron partitioning in continentally derived particulates, Chem. Geol., 214, 209–221, doi: 10.1016/j.chemgeo.2004.09.003, 2005.

Praharaj, T. and Fortin, D.: Determination of acid volatile sulfides and chromium reducible sulfides in Cu-Zn and Au mine tailings. Water, Air, & Soil Pollution, 155, 35–50, doi: 10.1023/B:WATE.0000026526.26339.c3, 2003.

Pyzik, A. J. and Sommer, S. E.: Sedimentary iron monosulfides: kinetics and mechanism of formation, Geochim. Cosmochim. Acta, 45, 687-698, doi: 10.1016/0016-7037(81)90042-9, 1981.

https://doi.org/10.5194/egusphere-2024-1942
Preprint. Discussion started: 17 July 2024
© Author(s) 2024. CC BY 4.0 License.

Reed, D. C., Slomp C. P., and Gustafsson, B. G.: Sedimentary phosphorus dynamics and the evolution of bottom-water hypoxia: A coupled benthic-pelagic model of a coastal system, Limnol. Oceanogr., 56, 1075–1092, doi: 10.4319/lo.2011.56.3.1075, 2011a.

Reed, D. C., Slomp, C. P., and de Lange, G.J.: A quantitative reconstruction of organic matter and nutrient diagenesis in Mediterranean Sea sediments over the Holocene, Geochim. Cosmochim. Acta, 75, 5540–5558, doi: 10.1016/j.gca.2011.07.002, 2011b.

Riedinger, N., Pfeifer, K., Kasten, S., Garming, J. F. L., Vogt, C., and Hensen, C.: Diagenetic alteration of magnetic signals by anaerobic oxidation of methane related to a change in sedimentation rate, Geochim. et Cosmochim. Acta, 69:16, 4117–4126, doi: 10.1016/j.gca.2005.02.004, 2005.

Riedinger, N., Brunner, B., Formolo, M. J., Solomon, E., Kasten, S., Strasser, M., and Ferdelman, T. G.: Oxidative sulfur cycling in the deep biosphere of the Nankai Trough, Japan, Geology, 38, 851–854, doi: 10.1130/G31085.1, 2010.

Riedinger, N., Formolo, M. J., Lyons, T. W., Henkel, S., Beck, A., and Kasten, S.: An inorganic geochemical argument for coupled anaerobic oxidation of methane and iron reduction in marine sediments, Geobiology, 12, 172-181, doi: 10.1111/gbi.12077, 2014.

Riedinger, N., Brunner, B., Krastel, S., Arnold, G. L., Wehrmann, L. M., Formolo, M. J., Beck, A., Bates, S. M., Henkel, S., Kasten, S., and Lyons, T. W.: Sulfur cycling in an iron oxide-dominated, dynamic marine depositional system: The Argentine continental margin, Front. Earth Sci., 5:33, doi: 10.3389/feart.2017.00033, 2017.

Roden, E. E. and Lovley, D. R.: Dissimilatory Fe(III) reduction by the marine microorganism *Desulfuromonas acetoxidans*, Appl. Environ. Microbiol., 59, 734-742, doi: 10.1128/aem.59.3.734-742.1993, 1993.

Rothe, M., Frederichs, T., Eder, M., Kleeberg, A., and Hupfer, M.: Evidence for vivianite formation and its contribution to long-term phosphorus retention in a recent lake sediment: a novel analytical approach, Biogeosciences, 11, 5169–5180, doi: bg-11-5169-2014, 2014.

Roy, M., Rouxel, O., Martin, J. B., and Cable, J. E.: Iron isotope fractionation in a sulfide-bearing subterranean estuary and its potential influence on oceanic Fe isotope flux, Chem. Geol., 300-301, 133-142, doi: 10.1016/j.chemgeo.2012.01.022, 2012.

Rullkötter, J.: Organic Matter: The driving force for early diagenesis, In: Schulz H.D., Zabel M. (eds) Marine Geochemistry. Springer, Berlin, Heidelberg. 10.1007/3-540-32144-6_4, 2006.

Schoenberg, R. and von Blanckenburg, F.: An assessment of the accuracy of stable Fe isotope ratio measurements on samples with organic and inorganic matrices by high-resolution multicollector ICP-MS. Int. J. Mass Spectrom. 242, 257–272, doi: 10.1016/j.ijms.2004.11.025, 2005.

Scholz, F., Severmann, S., McManus, J., Noffke, A., Lomnitz, U., and Hensen, C.: On the isotope composition of reactive iron in marine sediments: Redox shuttle versus early diagenesis, Chem. Geol., 389, 48-59, doi: 10.1016/j.chemgeo.2014.09.009, 2014.

Seeberg-Elverfeldt, J., Schlüter, M., Feseker, T., and Kölling, M.: Rhizon sampling of porewaters near the sediment-water interface of aquatic systems, Limnol. Oceanogr. Methods, 3, 361–371, doi: 10.4319/lom.2005.3.361, 2005.

https://doi.org/10.5194/egusphere-2024-1942
Preprint. Discussion started: 17 July 2024
© Author(s) 2024. CC BY 4.0 License.

Segarra, K. E. A., Comerford, C., Slaughter, J., and Joye, S. B.: Impact of electron acceptor availability on the anaerobic oxidation of methane in coastal freshwater and brackish wetland sediments, Geochim. Cosmochim. Acta, 115, 15-30, doi: 10.1016/j.gca.2013.03.029, 2013.

Severmann, S., Johnson, C. M., Beard, B. L., and McManus, J.: The effect of early diagenesis on the Fe isotope compositions of porewaters and authigenic minerals in continental margin sediments, Geochim. Cosmochim. Acta, 70, 2006–2022, doi: 10.1016/j.gca.2006.01.007, 2006.

Severmann, S., McManus, J., Berelson, W. M., and Hammond, D. E.: The continental shelf benthic iron flux and its isotope composition, Geochim. Cosmochim. Acta, 74, 3984-4004, doi: 10.1016/j.gca.2010.04.022, 2010.

Sieber, M., Conway, T. M., De Souza, G. F., Hassler, C. S., Ellwood, M. J., and Vance, D.: Isotopic fingerprinting of biogeochemical processes and iron sources in the iron-limited surface Southern Ocean, EPSL, 567, 116967, doi: 10.1016/j.epsl.2021.116967, 2021.

Sivan, O., Shusta, S. S., and Valentine, L.: Methanogens rapidly transition from methane production to iron reduction, Geobiology, 14:2, 190-203, doi: 10.1111/gbi.12172, 2016.

Staubwasser, M., von Blanckenburg, F., and Schoenberg, R.: Iron isotopes in the early marine diagenetic iron cycle, Geology, 34, 629–632, doi: 10.1130/G22647.1, 2006.

Stoll, M. H. C., Bakker, K., Nobbe, G. H., and Haese, R. R.: Continuous-flow analysis of dissolved inorganic carbon content in seawater, Anal. Chem., 73, 4111-4116, doi: 10.1021/ac010303r, 2001.

Tessier, A., Campbell, P. G. C., and Bisson, M.: Sequential extraction procedure for the speciation of particulate trace metals, Anal. Chem., 51, 844–851, doi: 10.1021/ac50043a017, 1979.

Thamdrup, B., Finster, K., Würgler, Hansen J., and Bak, F.: Bacterial disproportionation of elemental sulfur coupled to chemical reduction of iron or manganese, Appl. Environ. Microbiol., 59:1, 101-108, doi: 10.1128/aem.59.1.101-108.1993, 1993.

Thamdrup, B., Fossing, H., and Jørgensen, B. B.: Manganese, iron, and sulfur cycling in a coastal marine sediment, Aarhus Bay, Denmark, Geochim. Cosmochim. Acta, 58:23, 5115-5129, doi: 10.1016/0016-7037(94)90298-4, 1994.

Thiel, J., Byrne, J. M., Kappler, A., Schink, B., and Pester, M.: Pyrite formation from FeS and H_2S is mediated through microbial redox activity, PNAS, 116:14, 6897–6902, doi: 10.1073/pnas.1814412116, 2019.

Vuillemin, A., Friese, A., Wirth, R., Schuessler, J. A., Schleicher, A. M., Kemnitz, H., Lücke, A., Bauer, K. W., Nomosatryo, S., von Blanckenburg, F., Simister, R., Ordoñez, L. G., Ariztegui, D., Henny, C., Russell, J. M., Bijaksana, S., Vogel, H., Crowe, S. A., Kallmeyer, J., and the Towuti Drilling Project Science team: Vivianite formation in ferruginous sediments from Lake Towuti, Indonesia, Biogeosciences, 17, 1955–1973, doi: 10.5194/bg-17-1955-2020, 2020.

Wang, Y. and Van Capellen, P.: A multicomponent reactive transport model of early diagenesis: Application to redox cycling in coastal marine sediments, Geochim. Cosmochim. Acta, 60:16, 2993-3014, doi: 10.1016/0016-7037(96)00140-8, 1996.

Wedepohl, K. H.: Chemical composition and fractionation of the continental crust, Geologische Rundschau, 80, 207–223, doi: 10.1007/BF01829361, 1991.

https://doi.org/10.5194/egusphere-2024-1942
Preprint. Discussion started: 17 July 2024
© Author(s) 2024. CC BY 4.0 License.

Wersin, P., Höhener, P., Giovanoli, R., and Stumm, W.: Early diagenetic influences on iron transformations in a freshwater lake sediment, Chem. Geol., 90, 233-252, doi: 10.1016/0009-2541(91)90102-W, 1991.

Weyer, S. and Schwieters, J. B.: High precision Fe isotope measurements with high mass resolution MC-ICPMS, Int. J. Mass Spec., 226, 355–368, doi: 10.1016/S1387-3806(03)00078-2, 2003.

Whiticar, M. J.: Carbon and hydrogen isotope systematics of bacterial formation and oxidation of methane, Chem. Geol., 161: 291-314, doi: 10.1016/S0009-2541(99)00092-3, 1999.

Wieder, R. K., Lang, G. E., and Granus, V. A.: An evaluation of wet chemical methods for quantifying sulfur fractions in freshwater wetland peat, Limnol. Oceanogr., 30, 1109–1115, doi: 10.4319/lo.1985.30.5.1109, 1985.

Wiederhold, J. G.: Metal stable isotope signatures as tracers in environmental geochemistry, Environ. Sci. Technol., 49, 2606−2624, doi: 10.1021/es504683e, 2015.

Wiesli, R. A., Beard, B. L., and Johnson, C. M.: Experimental determination of Fe isotope fractionation between aqueous Fe(II), siderite and “green rust” in abiotic systems, Chem Geol., 211, 343-362, doi: 10.1016/j.chemgeo.2004.07.002, 2004.

Wunder, L. C., Breuer, I., Willis-Poratti, G., Aromokeye, D. A., Henkel, S., Richter-Heitmann, T., Yin, X., Friedrich, M. W.: Manganese reduction and microbial communities involved in Antarctic surface sediments from Potter Cove, Frontiers in Microbiology, 15, doi: 10.3389/fmicb.2024.1398021, 2024.

Yin, X., Zhou, G., Wang, H., Han, D., Maeke, M., Richter-Heitmann, T., Aromokeye, D., Zhu, Q., Nimzyk, R., Elvert, M., and Friedrich, M. W.: Unexpected carbon utilization activity of sulfate-reducing microorganisms in temperate and permanently cold marine sediments, ISME J., 18:1, 1-14, doi: 10.1093/ismejo/wrad014, 2024.

Yu, L., He, D., Yang, L., Rensing, C., Zeng, R. J., and Zhou, S.: Anaerobic methane oxidation coupled to ferrihydrite reduction by *Methanosarcina barkeri*, Sci. Total Environ., 844, 157235, doi: 10.1016/j.scitotenv.2022.157235, 2022.

Zhou, Z., Henkel, S., Kasten, S., and Holtappels, M.: The iron "redox battery" in sandy sediments: Its impact on organic matter remineralization and phosphorus cycling, Sci. Total Environ., 865, 161168, doi: 10.1016/j.scitotenv.2022.161168, 2023.

Zhou, Z., Waska, H., Henkel, S., Dittmar, T., Kasten, S., and Holtappels, M.: Iron promotes the retention of terrigenous dissolved organic matter in subtidal permeable sediments, Environ. Sci. Technol., 58, 14, 6204–6214, doi: 10.1021/acs.est.3c09531, 2024.

Zhuang, L., Tang, J., Wang, Y., Hu, M., and Zhou, S.: Conductive iron oxide minerals accelerate syntrophic cooperation in methanogenic benzoate degradation, J. Hazard Matter, 293, 37-45, doi: 10.1016/j.jhazmat.2015.03.039, 2015.